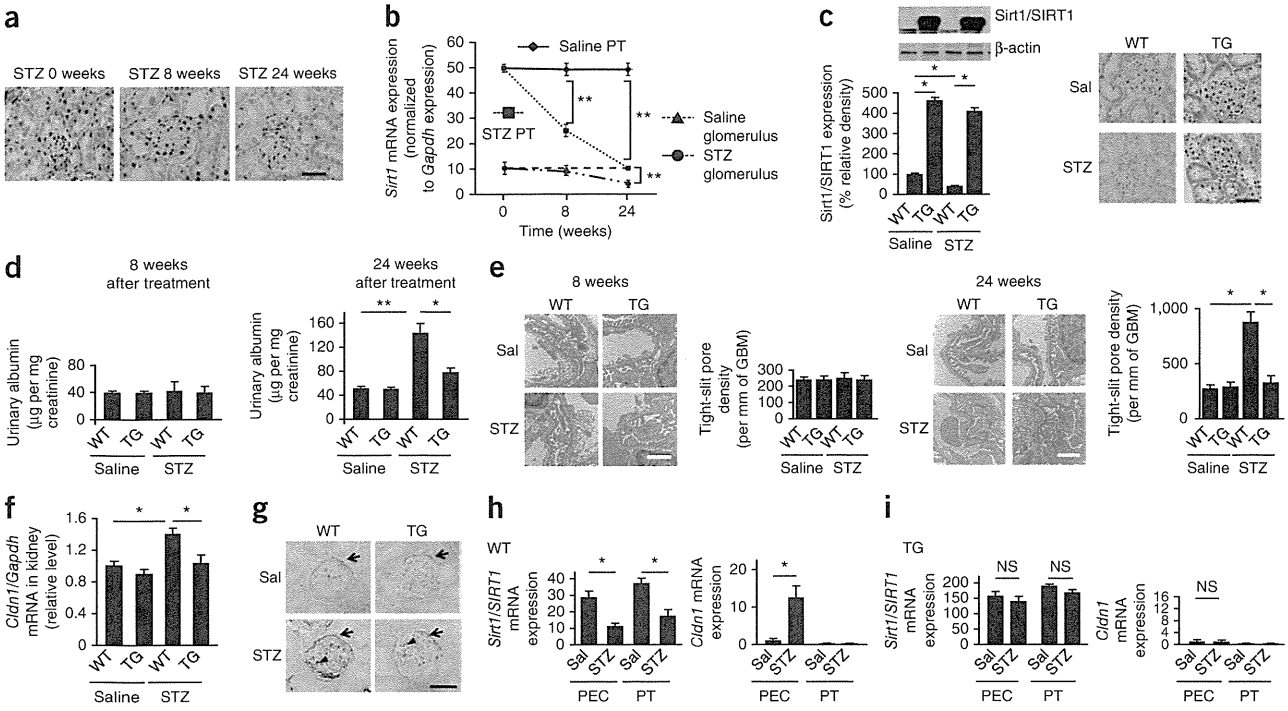

Figure 1 Alleviation of diabetes-induced albuminuria in TG mice with PT-specific overexpression of SIRT1. (**a**,**b**) Temporal changes in *Sirt1* expression 0, 8 and 24 weeks after STZ treatment in WT mice. (**a**) Immunostaining for Sirt1 in the kidney. Scale bar, 50 μm. (**b**) *Sirt1* mRNA expression levels normalized to *Gapdh* in PTs and glomeruli of saline- or STZ-treated mice. (**c**) Immunoblotting (left, top), immunostaining (right) and quantification (left, bottom) of Sirt1/SIRT1 expression in the kidneys of TG and WT mice treated with saline (Sal) or STZ and analyzed at 24 weeks after treatment. The Sirt1/SIRT1 band in TG mice consisted of a band for endogenous mouse Sirt1 (100 kDa) and one for Flag-tagged overexpressed human SIRT1 (101 kDa). Band intensities were normalized to β-actin. Scale bar, 50 μm. (**d**) Urinary albumin excretions at 8 (left) and 24 (right) weeks after STZ treatment. (**e**) Representative electron photomicrographs 8 (left) and 24 (right) weeks after STZ treatment. The bar graphs on the right show quantification of the tight-slit pore densities. Scale bars, 500 nm. GBM, glomerular basement membrane. (**f**) *Cldn1* mRNA levels. (**g**) Immunostaining for Claudin-1. Arrows indicate stained PECs. Arrowheads indicate stained cells in the glomeruli. Scale bar, 50 μm. (**h**,**i**) The expression of *Sirt1/SIRT1* (left) and *Cldn1* (right) mRNA in microdissected PECs and PTs of WT (**h**) and TG (**i**) mice treated with saline or STZ. $^*P < 0.05$, $^{**}P < 0.01$ (analysis of variance (ANOVA)). $n = 8$ mice per group. NS, not significant. All data are shown as the mean ± s.e.m.

overexpressed SIRT1 in PTs, but not glomeruli, using an antibody to Flag (**Supplementary Fig. 1c**). Immunoblotting, immunostaining and laser microdissection followed by RT-PCR all showed that the reduction in Sirt1 expression in wild-type (WT) mice at 24 weeks after STZ treatment was prevented in the TG mice, both in the PTs and glomeruli (**Fig. 1c** and **Supplementary Fig. 1a**,**b**). Plasma glucose concentrations increased in both WT and TG diabetic mice at 4 weeks after treatment with STZ, and the increase was sustained until 24 weeks. We euthanized mice 24 weeks after STZ treatment (**Supplementary Fig. 1d**). Plasma glucose concentrations did not differ between WT and TG mice at either 8 or 24 weeks after treatment (**Supplementary Fig. 1d**). Body weights, blood urea nitrogen and creatinine concentrations, creatinine clearance and kidney weights also did not differ between WT and TG mice (**Supplementary Fig. 1e–i**). Eight weeks after STZ treatment, urinary albumin excretion was unchanged among the four experimental groups of mice (**Fig. 1d**), although at 24 weeks after treatment, urinary albumin excretion in WT mice treated with STZ was greater than that in WT mice treated with saline (**Fig. 1d**). Urinary albumin excretion in STZ-treated TG mice was lower than that in STZ-treated WT mice (**Fig. 1d**). Mesangial matrix accumulations were not different between WT and TG mice treated with STZ (**Supplementary Fig. 1j**). As determined by electron microscopy (EM), the density of tight pores was not affected by STZ at 8 weeks after treatment among the four experimental groups of mice (**Fig. 1e**), although WT mice treated with STZ showed higher tight pore densities than WT mice treated with saline at 24 weeks. TG mice treated with STZ showed lower tight-pore densities than WT mice treated with STZ at 24 weeks (**Fig. 1e**).

Sirt1-dependent upregulation of Claudin-1 expression

To elucidate the molecular mechanisms underlying the amelioration of albuminuria by overexpression of SIRT1 in PTs, we performed DNA microarray analysis using microdissected glomerular regions to examine differences in gene expression between STZ-treated WT and TG mice. Using a Welch *t* test with a cutoff of $P < 0.05$, 26 genes showed a statistically significant upregulation of greater than fourfold in TG mice (**Supplementary Table 1**), and 29 genes showed downregulation in TG mice to ≤25% of the level in WT mice (**Supplementary Table 2**). We selected four upregulated genes and four downregulated genes with known functions and confirmed the differential expression of these genes by quantitative real-time RT-PCR using whole kidney samples (**Supplementary Fig. 2**). Only *Cldn1* (encoding Claudin-1) showed a marked reduction in mRNA level in TG mice treated with STZ compared to WT mice treated with STZ. In addition, among these eight genes, *Cldn1* has been reported to be the most related to the pathogenesis of albuminuria[21,22]. Therefore, we focused on changes in Claudin-1 expression.

Expression of *Cldn1* mRNA, a putative parietal epithelial cell (PEC)-specific marker[23–25], was higher in WT mice treated with STZ than

in saline-treated WT mice. We did not see this difference in TG mice (**Fig. 1f**). As determined by microarray analysis, no other isoforms of Claudin were upregulated or downregulated. Claudin-1 appeared to be expressed only in PECs of saline-treated WT mice, as determined by immunostaining (**Fig. 1g**). Claudin-1 levels were higher in STZ-treated WT mice than in saline-treated WT mice, and Claudin-1 extended ectopically in podocytes in STZ-treated WT mice (**Fig. 1g**). We did not see this difference in Claudin-1 levels in either PECs or podocytes in TG mice (**Fig. 1g**). Laser microdissection followed by real-time PCR revealed lower levels of *Sirt1* mRNA expression in PECs and PT cells of STZ-treated as compared to saline-treated WT mice (**Fig. 1h**). *Cldn1* mRNA expression was substantially higher in PECs of STZ-treated as compared to saline-treated WT mice, although we detected little *Cldn1* expression in PT cells of either group (**Fig. 1h**). In TG mice, *Sirt1/SIRT1* mRNA expression levels were unaffected by STZ in either PTs or PECs (**Fig. 1i**). We detected little expression of *Cldn1* in PTs and PECs of TG mice, and its expression in these regions was unaffected by STZ (**Fig. 1i**). Using immunogold EM of the foot processes of podocytes, we observed no gold particles for Claudin-1 in saline-treated WT mice, whereas we observed large numbers in STZ-treated WT mice. We did not see this difference in TG mice (**Supplementary Fig. 3a–c**). Collectively these findings suggest that Sirt1 overexpression in PTs alters Claudin-1 expression in PECs and podocytes but not PT cells.

Effects of Claudin-1 expression in podocytes

To examine the effects of Claudin-1 on albuminuria, we transferred a construct containing the *Cdn1* gene inserted downstream of a podocyte-specific promoter, a 2.5-kb fragment of the *NPHS2* (podocin) promoter, into WT mice with the aid of a hemagglutinating virus of the Japan envelope vector[26]. Injection of the *Cldn1* gene driven by a *NPHS2* promoter successfully upregulated Claudin-1 expression in podocytes (**Fig. 2a**). This gene transfer induced albuminuria in WT mice and aggravated albuminuria in STZ-treated mice (**Fig. 2b**). These effects were accompanied by greater podocyte effacement (**Fig. 2c**).

The β-catenin–Snail pathway has a role in the pathogenesis of albuminuria[27], and Claudin-1 reportedly activates the β-catenin–Snail pathway in colon epithelial cells[28]. Thus we examined whether Claudin-1 activates the β-catenin–Snail pathway in podocytes. Transfer of the *Cldn1* gene upregulated both *Ctnnb1* (β-catenin) and *Snai1* (Snail) mRNA levels concomitantly with downregulation of the mRNAs for the slit membrane protein podocin (*Nphs2*) and

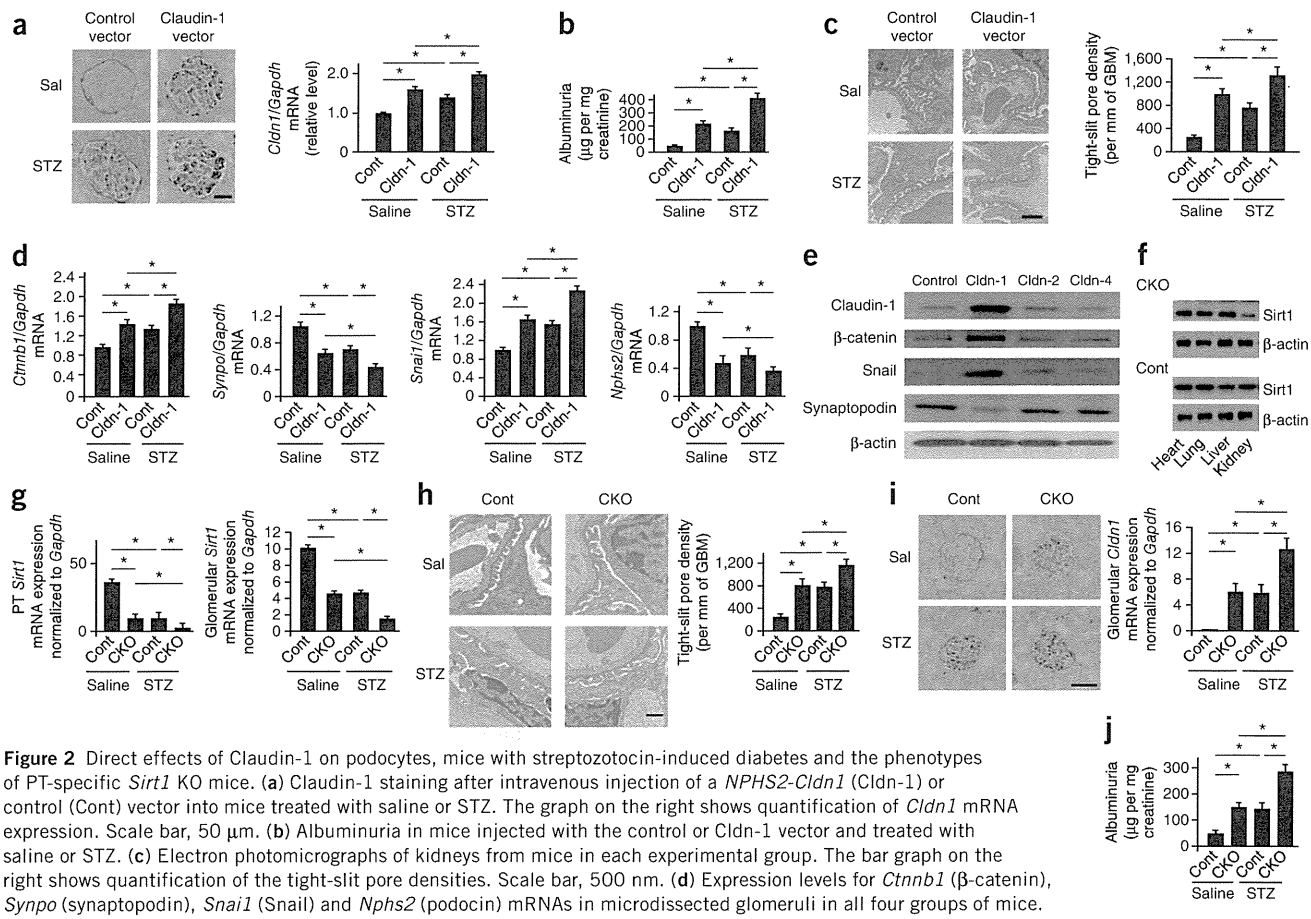

Figure 2 Direct effects of Claudin-1 on podocytes, mice with streptozotocin-induced diabetes and the phenotypes of PT-specific *Sirt1* KO mice. (**a**) Claudin-1 staining after intravenous injection of a *NPHS2-Cldn1* (Cldn-1) or control (Cont) vector into mice treated with saline or STZ. The graph on the right shows quantification of *Cldn1* mRNA expression. Scale bar, 50 μm. (**b**) Albuminuria in mice injected with the control or Cldn-1 vector and treated with saline or STZ. (**c**) Electron photomicrographs of kidneys from mice in each experimental group. The bar graph on the right shows quantification of the tight-slit pore densities. Scale bar, 500 nm. (**d**) Expression levels for *Ctnnb1* (β-catenin), *Synpo* (synaptopodin), *Snai1* (Snail) and *Nphs2* (podocin) mRNAs in microdissected glomeruli in all four groups of mice. (**e**) Immunoblotting analysis for the expression of Claudin-1, β-catenin, Snail and synaptopodin in cultured podocytes transfected with expression vectors for Claudin-1, Claudin-2 (Cldn-2) or Claudin-4 (Cldn-4) or the empty vector pcDNA3 (control). (**f**) Immunoblotting analysis for Sirt1 expression in the heart, lung, liver and kidney of CKO and control (Cont) mice. (**g**) Expression of *Sirt1* in PTs (left) and glomeruli (right) of CKO and control mice. (**h**) Electron photomicrographs of kidneys from STZ-treated CKO and control mice. The bar graph on the right shows quantification of the tight-slit pore densities. Scale bar, 500 nm. (**i**) Immunostaining for Claudin-1 in kidneys (left) and *Cldn1* mRNA expression in microdissected glomeruli (right) from the four groups of mice. Scale bar, 50 μm. (**j**) Albuminuria in each experimental group. $^*P < 0.05$ (ANOVA). $n = 8$ mice per group. All data are shown as the mean ± s.e.m.

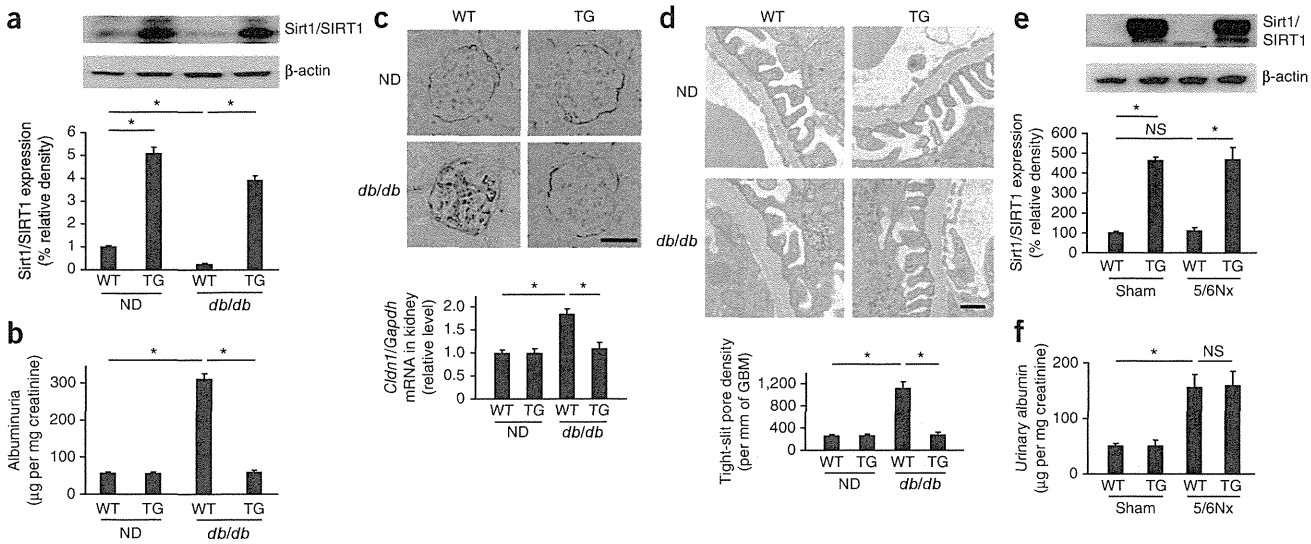

Figure 3 PT-specific SIRT1 overexpression alleviates diabetic albuminuria in *db/db* mice but not 5/6Nx mice. (**a**) Immunoblotting for Sirt1/SIRT1 in the kidneys of TG mice and WT littermates crossed with *db/db* or ND mice. The graph on the bottom shows the results of the densitometry analysis of band intensities. (**b**) Albuminuria in WT ND, TG ND, WT *db/db* and TG *db/db* mice. (**c**) Immunostaining for Claudin-1 in kidneys from each experimental group. The bar graph on the bottom shows quantification of *Cldn1* mRNA expression. Scale bar, 50 μm. (**d**) Electron photomicrographs of kidneys from mice in each group (top) and quantification of the tight-slit pore densities (bottom). Scale bar, 500 nm. (**e**) Immunoblotting for Sirt1/SIRT1 in the kidneys of TG and WT mice after 5/6Nx or sham operation. The bar graph on the bottom shows the densitometry analysis of band intensities. (**f**) Albuminuria in TG and WT mice after 5/6Nx or sham operation. $^*P < 0.05$ (ANOVA). NS, not significant. $n = 8$ mice per group. All data are shown as the mean ± s.e.m.

the actin-binding protein synaptopodin (*Synpo*) in microdissected glomeruli (**Fig. 2d**). Overexpression of Claudin-1 was also associated with increased expression of β-catenin and Snail and downregulated synaptopodin expression in cultured podocytes (**Fig. 2e**). Collectively these findings suggest that expression of Claudin-1 in podocytes induces podocyte effacement and leads to albuminuria, presumably through the activation of β-catenin–Snail signaling.

Deficiency of Sirt1 in PTs causes albuminuria

To confirm the role of PT Sirt1 in albuminuria in diabetes, we created mice deficient in *Sirt1* specifically in PTs (conditional knockout (CKO) mice) by crossing *Sirt1*$^{flox/flox}$ mice on a C57BL/6J background with γ-glutamyl transpeptidase(γ-GT)-Cre mice. CKO mice showed specific loss of Sirt1 expression in the kidney (**Fig. 2f**). Immunofluorescence staining revealed that control littermates aged 8 weeks expressed Sirt1 in the glomeruli and tubules in kidney tissues. In CKO mice, we observed almost complete elimination of Sirt1 expression in the tubules, whereas glomerular expression was unaffected, denoting tubular-specific knockout of *Sirt1* (**Supplementary Fig. 4a**).

We then compared phenotypes in 32-week-old mice (24 weeks after saline or STZ treatment). Microdissection followed by real-time PCR revealed lower PT *Sirt1* expression levels in CKO mice than in control mice (**Fig. 2g**). In addition, *Sirt1* expression levels were also lower in glomeruli of CKO mice (**Fig. 2g**). *Sirt1* expression levels in PTs and glomeruli were lower in control mice treated with STZ and CKO mice treated with saline than in control mice treated with saline. Sirt1 expression in CKO mice treated with STZ was lower than that in CKO mice treated with saline and that in STZ-treated control mice (**Fig. 2g**). The results of immunofluorescence staining (**Supplementary Fig. 4a**) were consistent with those of real-time PCR. As determined by EM, the density of tight pores was higher in STZ-treated control mice and saline-treated CKO mice than in saline-treated control mice, and we observed an even higher tight pore density in STZ-treated CKO mice (**Fig. 2h**). Immunostaining (**Fig. 2i**), real-time PCR after laser microdissection (**Fig. 2i**) and immunogold EM (**Supplementary Fig. 4b**) revealed higher levels of Claudin-1 expression in STZ-treated control mice and saline-treated CKO mice compared with saline-treated control mice, an effect that was further enhanced in STZ-treated CKO mice. Urinary albumin excretion was greater in STZ-treated control mice and saline-treated CKO mice than in saline-treated control mice and was even greater in STZ-treated CKO mice (**Fig. 2j**). These data from PT-specific *Sirt1*-deficient mice confirm the pivotal role of endogenous PT Sirt1 in maintaining glomerular structure and function during the initiation of albuminuria in diabetes, as well as in normal conditions.

SIRT1 overexpression in obese and nephrectomized mice

We further investigated the effects of SIRT1 overexpression in PTs in another diabetic model and 5/6 nephrectomized (5/6Nx) mice. We crossed our *SIRT1* TG mice with obese *db/db* mice and produced *SIRT1* TG *db/db* mice. Plasma glucose concentrations and body weights were substantially higher in WT *db/db* mice and TG *db/db* mice as compared to nondiabetic (ND) mice. Plasma glucose concentrations were elevated by 8 weeks of age in both WT *db/db* and TG *db/db* mice, and this elevation was sustained until 32 weeks of age (**Supplementary Fig. 4c**). Body weights, blood urea nitrogen and creatinine concentrations, creatinine clearance and kidney-to–body weight ratios did not differ between the WT *db/db* and TG *db/db* groups (**Supplementary Fig. 4d–h**). SIRT1 expression in WT *db/db* mice was lower than in WT ND mice, but there was no significant difference in SIRT1 expression levels between TG ND mice and TG *db/db* mice (**Fig. 3a**). Urinary albumin excretion, Claudin-1 levels and the density of tight pores did not differ between 32-week-old TG ND mice and WT ND mice. However, these parameters were greater in WT *db/db* mice than in either type of ND mice at 32 weeks of age, when glomerular lesions were evident. In TG *db/db* mice, we

observed no such difference (**Fig. 3b–d**). Periodic acid-Schiff (PAS) staining revealed an increase in mesangial matrix accumulation in the diabetic groups, but there was no difference in accumulation between WT *db/db* and TG *db/db* mice (**Supplementary Fig. 4i**).

To explore the role of renal tubular Sirt1 in non-diabetes related albuminuria, we performed similar experiments using 5/6Nx mice[29]. Twenty-four weeks after nephrectomy, the expression of Sirt1 was unchanged in these mice, and PT-specific *SIRT1* TG mice expressed high levels of SIRT1 in the kidney (**Fig. 3e**). The 5/6Nx mice exhibited albuminuria at a level that was similar to that in STZ-treated WT mice. However, PT-specific SIRT1 overexpression could not prevent albuminuria in 5/6Nx mice (**Fig. 3f**). Collectively, these data indicate that the effect of PT Sirt1 in preventing albuminuria is a diabetes-specific event.

Epigenetic mechanism of SIRT1-induced Claudin-1 upregulation

We further explored the mechanism regulating Claudin-1 expression using human-derived renal epithelial (HRE) cells, as this cell line expresses Claudin-1 and has a similar phenotype to that of PECs. SIRT1 expression decreased and Claudin-1 expression increased as glucose concentration increased (**Fig. 4a**). Transfection of cells with increasing amounts of SIRT1 expression vectors resulted in downregulation of Claudin-1 expression (**Fig. 4b**). SIRT1 overexpression blunted the upregulation of Claudin-1 by glucose (**Fig. 4b**). We then investigated

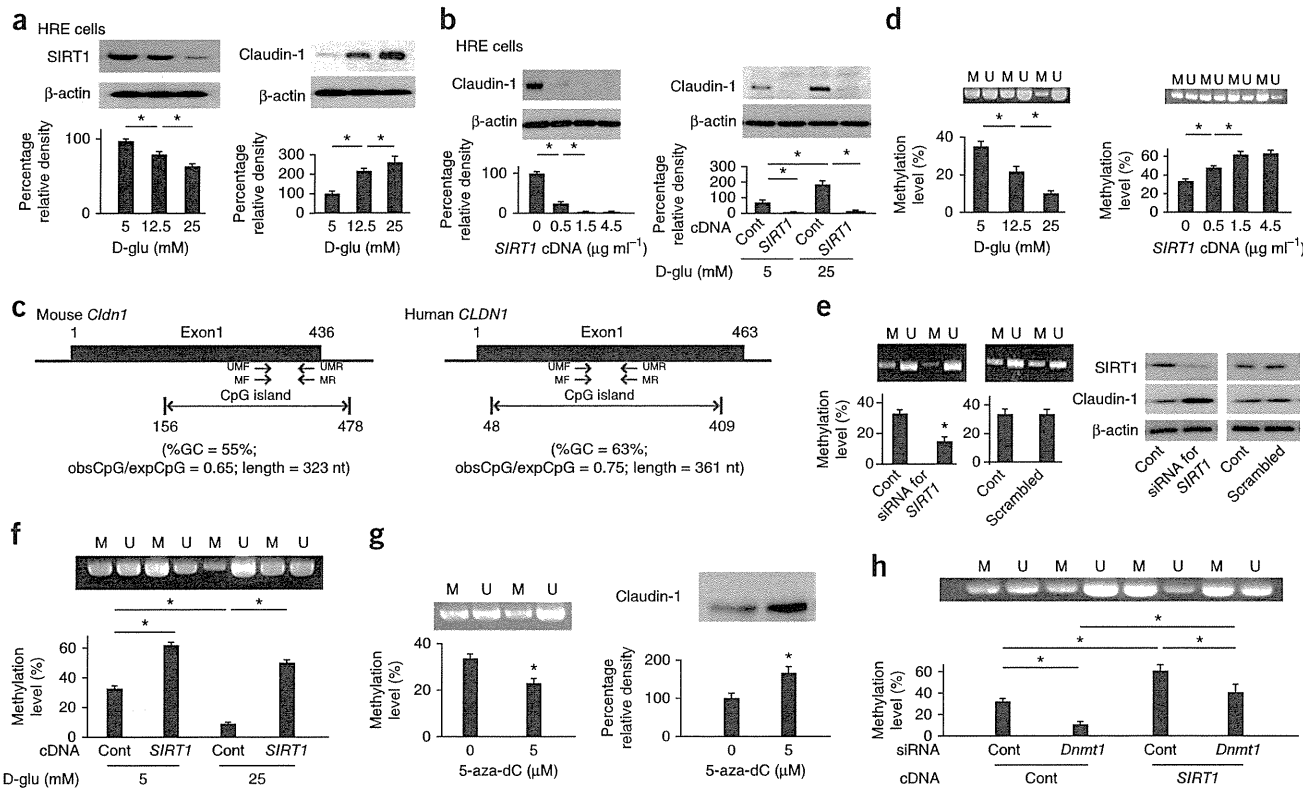

Figure 4 Epigenetic regulation of *Cldn1* gene expression by SIRT1. (**a**) Effects of glucose concentration on the expression of SIRT1 (left) and Claudin-1 (right). D-glu, D-glucose (glucose). (**b**) Effects of SIRT1 overexpression (left) and the combined effects of glucose and SIRT1 overexpression (right) on Claudin-1 expression. (**c**) CpG islands and positions of forward (F) and reverse (R) primers for methylated (MF and MR) and unmethylated (UMF and UMR) genes on mouse (left) and human (right) *CLDN1*. ObsCpG, observed CpG islands; expCpG, expected CpG islands. (**d**) Effects of glucose concentration (left) and SIRT1 overexpression (right) on *Cldn1* gene methylation. M, methylated; U, unmethylated. (**e**) Effects of transfection with siRNA for *SIRT1* on methylation of *Cldn1* (left) and expression of Claudin-1 (right). (**f**) Combined effects of glucose and SIRT1 overexpression on *Cldn1* gene methylation. (**g**) Methylation of *Cldn1* (left) and Claudin-1 protein expression (right) after treatment with the Dnmt inhibitor 5-aza-dC. (**h**) Methylation of *Cldn1* after transfection with or without SIRT1 expression vectors or *Dnmt1* siRNA. (**i**) ChIP assays using HRE cells cultured with sirtinol (S; 20 mM) or vehicle (control; C). Antibodies to acetylated histone 4 (H4ac), acetylated histone 3 (H3ac), H4K20me2 and H3K9me2 were used. (**j**) *Cldn1* CpG methylation in the kidneys of TG mice treated with or without STZ. Left, methylation-specific PCR and real-time methylation-specific PCR using microdissected PECs. Right, *Cldn1* mRNA expression in PECs. $^*P < 0.05$ (ANOVA). $n = 5$ independent experiments. All data are shown as the mean ± s.e.m.

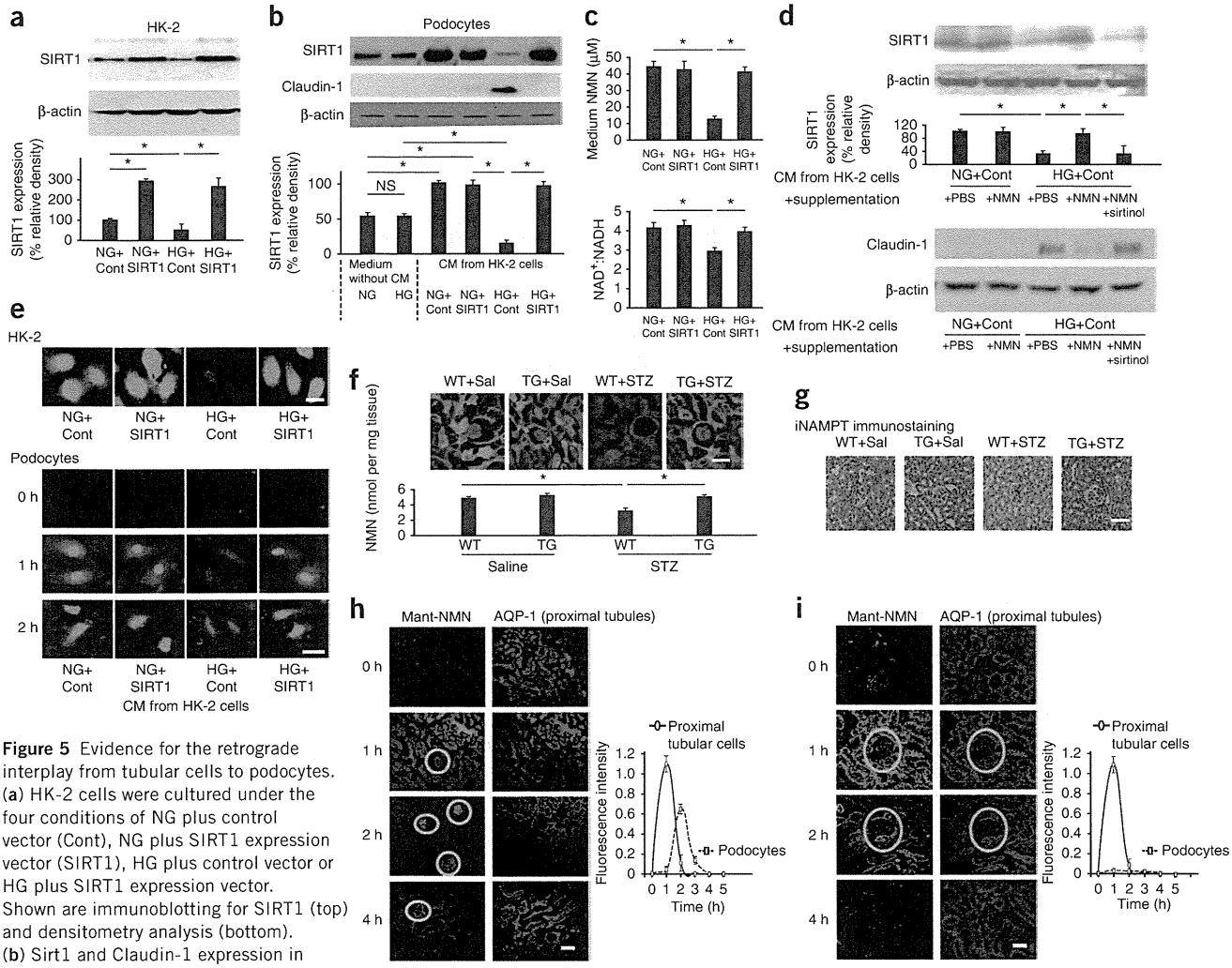

Figure 5 Evidence for the retrograde interplay from tubular cells to podocytes. (**a**) HK-2 cells were cultured under the four conditions of NG plus control vector (Cont), NG plus SIRT1 expression vector (SIRT1), HG plus control vector or HG plus SIRT1 expression vector. Shown are immunoblotting for SIRT1 (top) and densitometry analysis (bottom). (**b**) Sirt1 and Claudin-1 expression in podocytes cultured in CM from each of the four experimental conditions described in **a** or in NG or HG conditions without CM. (**c**) NMN concentrations (top) and the NAD^+-to-NADH ratio (lower) of each CM. (**d**) Sirt1 (top) and Claudin-1 (bottom) expression in podocytes cultured in each CM supplemented with NMN, PBS or sirtinol. (**e**) Intracellular autofluorescence of NMN in HK-2 cells (top) and podocytes (bottom) at 0, 1 and 2 h after CM transfer. CM were from the four conditions of HK-2 cell culture media. Scale bars, 20 μm. (**f**,**g**) Tissue NMN concentrations (**f**) and intracellular-type NAM phosphoribosyltransferase (iNAMPT) immunostaining (**g**) of kidneys from PT-specific *SIRT1* TG mice and WT littermates 24 weeks after treatment with saline or STZ. Scale bars, 50 μm. (**h**,**i**) Representative confocal images of Mant fluorescence in normal (**h**) and PT-specific *Sirt1*-deficient (**i**) mice. Mant-NMN (green, left) was detected at 0, 1, 2 and 4 h after injection. Sequential sections were stained with antibody to aquaporin 1 (AQP-1) (right). Glomeruli are indicated by circles. Temporal profiles of the mean Mant-NMN intensity in tubular and podocyte regions are shown in the graphs on the left. Scale bars, 50 μm. $^*P < 0.05$ (ANOVA). NS, not significant. $n = 5$ independent experiments. All data are shown as the mean ± s.e.m.

the epigenetic mechanisms for regulating Claudin-1 expression[30]. A computer search indicated that CpG islands, a target for methylation, reside within the *CLDN1* genes of both mice and humans (**Fig. 4c**). Methylation analysis revealed that the amount of methylated CpG decreased with increasing glucose concentration in concert with upregulation of Claudin-1 (**Fig. 4d**). The transfection of cells with increased concentrations of SIRT1 expression vectors induced hypermethylation of the *Cldn1* gene in concert with downregulation of Claudin-1 (**Fig. 4d**). Transfection of cells with an siRNA for *SIRT1* induced hypomethylation of the *Cldn1* gene and upregulated Claudin-1 expression (**Fig. 4e**). SIRT1 overexpression blunted the hypomethylation of the *Cldn1* gene CpG islands that was induced by glucose (**Fig. 4f**).

Treatment of cells with 5-aza-dC, a DNA methyltransferase (Dnmt) inhibitor, reduced the level of methylation of the *Cldn1* gene and increased Claudin-1 protein levels (**Fig. 4g**). The methylation of the *Cldn1* CpG region that was induced by overexpression of SIRT1 was suppressed by cotransfection of cells with an siRNA for *Dnmt1* (**Fig. 4h**) but not by cotransfection of cells with siRNAs for *Dnmt3a* and *Dnmt3b* (**Supplementary Fig. 5a,b**). In an inactivation model of gene expression, histone deacetylation induces histone methylation, which leads to the recruitment of Dnmt[31,32]. We examined chromatin modification status by chromatin immunoprecipitation (ChIP) assays to confirm the molecular events in the CpG islands within the *Cldn1* gene[33,34]. Acetylation of histones H3 and H4 was greater in both CpG and non-CpG regions in cells treated with sirtinol, a Sirt1 inhibitor, than in untreated cells (**Fig. 4i**). Histone H3 Lys9 dimethylation (H3K9me2) in the CpG region was decreased by sirtinol, although H4K20me2 was unaffected by sirtinol treatment (**Fig. 4i**). These results suggest

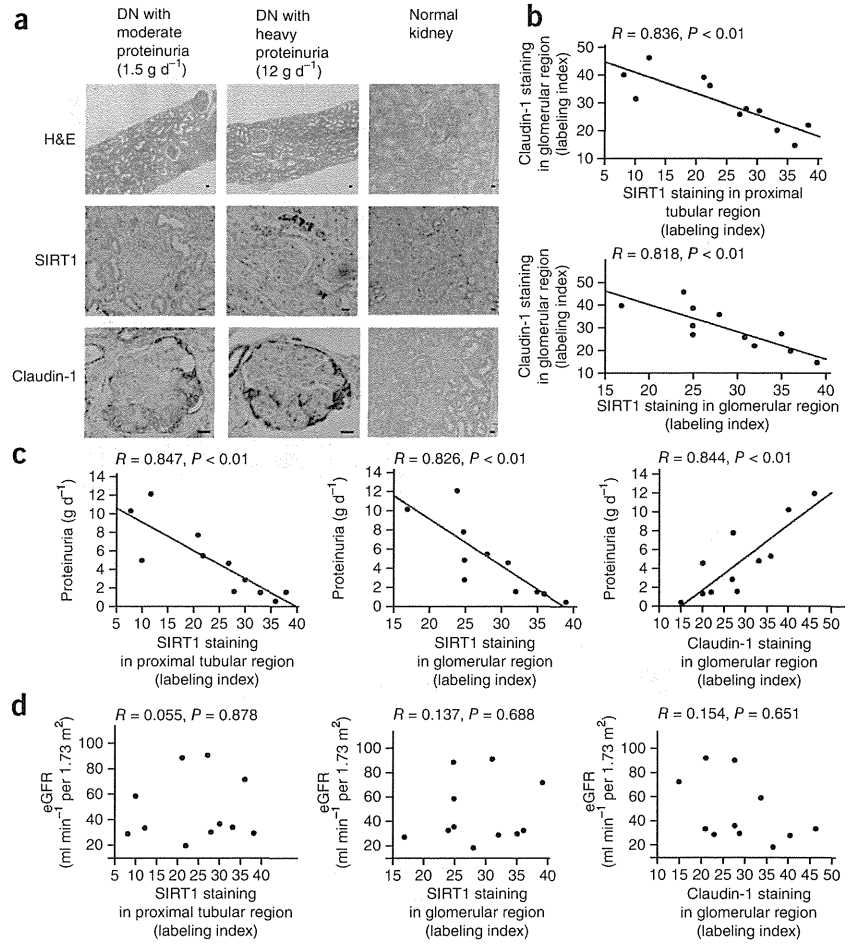

Figure 6 Immunostaining for glomerular SIRT1 or Claudin-1 in human renal biopsy specimens. (**a**) Representative photomicrograph of H&E staining or immunostaining for SIRT1 and Claudin-1 in needle renal biopsy specimens of subjects with diabetic nephropathy (DN) (**Supplementary Table 3**) and a control specimen. Scale bars, 50 nm. (**b**) The relationship between immunostaining for Claudin-1 and SIRT1 in the proximal tubular (top) and glomerular (bottom) regions in renal biopsy specimens from subjects with DN. $n = 11$ subjects. (**c**) The relationships between proteinuria and immunostaining for proximal tubular SIRT1 (left), glomerular SIRT1 (middle) and Claudin-1 (right). $n = 11$ subjects. (**d**) The relationships between eGFR and immunostaining for proximal tubular SIRT1 (left), glomerular SIRT1 (middle) and Claudin-1 (right). $n = 11$ subjects. *P* values throughout the figure were determined by Pearson's *R* test.

that SIRT1 deacetylated the H3 and H4 histones in both CpG and non-CpG regions and enhanced H3K9me2 in CpG regions (**Fig. 4i**). They also indicate that Claudin-1 expression is regulated epigenetically through deacetylation of histones H3 and H4 by SIRT1, with subsequent CpG methylation of the *Cldn1* gene by recruited *Dnmt1*.

We confirmed these epigenetic changes in PECs microdissected from STZ-treated *SIRT1* TG mice. Diabetes-induced hypomethylation of *Cldn1* CpG regions and SIRT1 overexpression led to higher levels of methylation of these regions (**Fig. 4j**). In parallel with these epigenetic changes, the levels of *Cldn1* mRNA expression were higher in STZ-treated WT mice than in STZ-treated TG mice (**Fig. 4j**). We obtained more quantitative results by bisulfite sequencing using microdissected PECs (**Supplementary Fig. 5c,d**).

Interaction between PT cells and podocytes through NMN

Our data indicated that the phenotype changes in PT cells affected contiguous cells, including podocytes. We examined this interaction between PT cells and podocytes in conditioned medium (CM) experiments. We transfected a human renal PT cell line, HK-2, cultured in either normal-glucose (NG) or high-glucose (HG) conditions, with SIRT1 expression vectors (**Fig. 5a**). We obtained CM from these cells and treated podocytes with or without these conditioned media. Podocytes cultured without CM expressed Sirt1 protein but had undetectable levels of Claudin-1 protein. In the absence of CM, HG culture conditions did not change the levels of these molecules. However, CM from HK-2 cells cultured in NG conditions induced higher levels of Sirt1 expression in podocytes. Exposure of podocytes to CM from HK-2 cells cultured in HG conditions downregulated Sirt1 and upregulated Claudin-1 in podocytes. These effects were diminished in podocytes exposed to CM from HK-2 cells transfected with the SIRT1 expression vector and cultured in HG conditions (**Fig. 5b**). Thus, the CM from HK-2 cells contained some factor that was responsible for the alteration of Sirt1 expression in podocytes.

Nicotinic acid metabolites are candidates for this effect because they are related to Sirt1 expression[35] and activity[36,37]. In this metabolic pathway, nicotinamide (NAM) is converted into NMN by intracellular-type NAM phosphoribosyltransferase. NMN is further converted into NAD^+ by nicotinamide mononucleotide adenylyl transferase. NAD^+ is then converted into NAM by Sirt1, forming a metabolic loop[36,38]. In our culture system, NMN concentrations and the NAD^+-to-NADH ratio were lower in CM from HK-2 cells cultured in the HG condition than in CM from HK-2 cells cultured in the NG condition. We did not observe such a difference in CM from *SIRT1*-transfected HK-2 cells (**Fig. 5c**). Exogenous supplementation of NMN into CM from HK-2 cells cultured in the HG condition induced higher levels of Sirt1 and lower levels of Claudin-1 in podocytes. Sirtinol abrogated these effects of NMN treatment (**Fig. 5d**). We did not observe these molecular changes when we used mannitol in the place of glucose, indicating that osmotic changes had no effects (**Supplementary Fig. 6a–f** and **Supplementary Results**). Collectively these findings suggest that Sirt1 prevented the HG-induced decrease in NMN and NAD^+ concentrations in CM, which could have contributed, at least in part, to the changes in Sirt1 expression and probably the subsequent alteration of Claudin-1 expression in podocytes.

We then measured NMN concentrations inside the cells in CM experiments. We detected NMN photoactivated by pretreatment with perchloric acid and acetophenone at high temperature[39] in HK-2 cells (**Fig. 5e**). HK-2 cells cultured in HG contained lower concentrations of NMN than those cultured in NG (**Fig. 5e**). This difference was reversed in HK-2 cells transfected with the SIRT1 expression vector. In podocytes, basal concentrations of NMN were almost undetectable (**Fig. 5e**). One and two hours after exposure to NG CM, NMN concentrations

inside podocytes were higher. The NMN concentration was low when we treated podocytes with HG CM but was higher in podocytes treated with CM from *SIRT1*-transfected HK-2 cells (**Fig. 5e**). These data indicate that NMN synthesized and secreted by HK-2 cells was taken up by podocytes. Next, we directly measured tissue NMN concentrations in kidneys using this method. We detected NMN mainly in tubular regions (**Fig. 5f**), probably because of the high expression levels of the NMN-producing enzyme iNampt (**Fig. 5g**). NMN levels were lower in WT mice treated with STZ than in WT mice treated with saline, and this difference was less apparent in *SIRT1* TG mice (**Fig. 5f**). We consistently saw weaker immunostaining for iNampt in STZ-treated compared with saline-treated WT mice, whereas we saw stronger immunostaining in STZ-treated compared with saline-treated TG mice (**Fig. 5g**). Similarly, NMN concentrations were lower in STZ-treated control mice and saline-treated CKO mice than in saline-treated control mice and were even lower in STZ-treated CKO mice (**Supplementary Fig. 6g**). Immunostaining for iNampt was weaker in STZ-treated control mice and saline-treated CKO mice than in saline-treated control mice and was even weaker in STZ-treated CKO mice (**Supplementary Fig. 6h**). These results suggest that iNampt levels are affected, at least in part, by glucose or the Sirt1-determined tissue NMN concentrations around PTs, which regulate Sirt1 and Claudin-1 expression levels in podocytes.

To confirm a role for NMN in the progression of diabetes-induced albuminuria, we examined the effects of FK866, an inhibitor of iNampt. FK866 at the dose of 30 mg per kg body weight in 8-week-old male WT C57BL/6J mice decreased NMN concentrations (**Supplementary Fig. 7a**), leading to higher levels of Claudin-1 expression (**Supplementary Fig. 7b**) and albuminuria (**Supplementary Fig. 7c**). EM revealed that FK866 induced higher tight-slit pore density and Claudin-1 levels in podocytes (**Supplementary Fig. 7d,e**).

Our data imply a pivotal role for the molecular interplay between iNampt and NMN in PTs and Sirt1 and Claudin-1 in podocytes in diabetes-induced albuminuria. We thus investigated retrograde interplay from tubular cells to podocytes in an *in vivo* system. N-methylanthraniloyl (Mant)-NMN is an autoimaging substance that cannot be synthesized endogenously[40,41]. One hour after injection into the renal artery in 8-week-old control mice, Mant-NMN accumulated in tubules, and 2 h after injection, its accumulation could be detected in glomeruli (**Fig. 5h**). These temporal changes in the localization of Mant-NMN strongly suggested that NMN was taken up by tubular cells and thereafter delivered into glomeruli. In CKO mice that lack the ability to supply NMN to glomeruli from proximal tubules, the late peak in podocytes was almost abolished (**Fig. 5i**). This result supports the hypothesis that the NMN accumulation in podocytes is derived from proximal tubules and not from slow accumulation in glomeruli. However, we need to further investigate the detailed mechanisms underlying NMN secretion or absorption. Presumably, NMN absorption in podocytes will depend on nucleotide receptors such as P2X or P2Y[42].

SIRT1 and Claudin-1 expression in human renal biopsy samples

We evaluated renal the expression of SIRT1 and Claudin-1 in human specimens from 11 subjects with diabetes (**Supplementary Table 3**). SIRT1 expression in both PTs and glomerular regions was lower, and Claudin-1 expression in the glomerular region was higher, in the kidneys of subjects with heavy proteinuria (12 g d^{-1}) compared with those with moderate proteinuria (1.5 g d^{-1}) (**Fig. 6a**). Claudin-1 expression was negatively correlated with SIRT1 expression in both PTs and glomerular regions (**Fig. 6b**).

Among several clinical parameters, only proteinuria was correlated with both PT and glomerular SIRT1 immunostaining, as well as with glomerular Claudin-1 immunostaining (**Fig. 6c**). There were no correlations between estimated glomerular filtration rate (eGFR) and immunostaining patterns for either protein (**Fig. 6d**).

DISCUSSION

Our data reveal that reduced Sirt1 expression in PTs leads to reduced Sirt1 levels and higher Claudin-1 levels in glomeruli, leading to the initiation of albuminuria in a diabetic mouse model. These findings indicate a protective role for PT Sirt1 against albuminuria that is specific for diabetes-induced albuminuria.

We also show direct epigenetic regulation of *Cldn1* gene expression by SIRT1. The important role of Dnmt1 in SIRT1-induced gene methylation in the present study is consistent with a recent study showing that Sirt1 directly deacetylates and activates Dnmt1 (ref. 43). The results in our PT-specific genetically engineered mice imply that the molecular changes in PTs induced the phenotype changes in glomeruli and podocytes.

We also show a role for NMN as a candidate mediator of the interplay between PT cells and podocytes. We confirmed this retrograde interplay by tracing photoactivated labeled NMN both *in vitro* and *in vivo*. Our data suggest that NMN derived from PT cells is absorbed by podocytes; however, more work will be needed to confirm this hypothesis (**Supplementary Fig. 8**).

We also show that expression of SIRT1 and Claudin-1 is correlated with levels of proteinuria in human renal biopsy samples from subjects with diabetes. Because neither of our diabetic mouse models developed severe diabetic nephropathy, we should interpret the present data carefully. In addition, the mechanisms regulating NMN concentrations in PTs on the basis of glucose condition or Sirt1 expression level remain unclear. However, because the clinical data are consistent with the results obtained from mouse models, we suggest that an initial downregulation of Sirt1 expression in PTs, which is followed by downregulation of Sirt1 and upregulation of Claudin-1 in glomeruli, has a role in the initial changes in diabetes-induced albuminuria[44]. The results of this study could contribute to new therapeutic strategies to prevent diabetes-induced albuminuria.

NMN, an intermediate of nicotinic acid metabolism, is synthesized by iNAMPT. In the diabetic milieu, reduced expression of Sirt1 causes downregulation of iNAMPT, presumably by direct transcriptional mechanisms[45]. This decrease in iNAMPT leads to the reduction in the levels of NMN secreted from tubular cells. Although it would be diluted by urine during retrograde flow, in the microenvironment near podocytes inside the Bowman's capsule, the continuous secretion of NMN by proximal tubular cells or PECs would maintain a certain level of NMN around podocytes. This level might decrease in the diabetic milieu, although the direct measurement of local NMN concentrations remains to be investigated. Further, a decrease in NMN taken up in podocytes downregulates Sirt1, which epigenetically increases Claudin-1. Claudin-1 is reported to activate the β-catenin–Snail pathway[28], and as demonstrated in the present study, this activation would change glomerular barrier function through downregulating synaptopodin or podocin expression in podocytes[27]. The detailed mechanisms of these molecular interplays in podocytes warrant further investigations.

METHODS

Methods and any associated references are available in the online version of the paper.

Note: Any Supplementary Information and Source Data files are available in the online version of the paper.

ACKNOWLEDGMENTS

We thank P. Mundel (Division of Nephrology, Massachusetts General Hospital and Harvard Medical School) and K. Asanuma (Division of Nephrology, Department of Internal Medicine, Juntendo University Faculty of Medicine) for providing cultured podocytes. We also thank S.J. Shankland and C. Campbell (Division of Nephrology, University of Washington) for providing culture PECs. This work was supported by the Scientific Research Fund of the Ministry of Education, Culture, Sports, Science and Technology of Japan (grant 22790800).

AUTHOR CONTRIBUTIONS

K. Hasegawa, S.W., L.G. and H.I. designed the experiments and the study. K. Hasegawa, P.S., Y.S. and E.K. collected data or performed experiments for the study. K. Hasegawa, S.W., P.S., H.M., K.F., K. Hosoya, M.K., Y.K., T.K., H.T., K. Hayashi, L.G. and H.I. analyzed the data and contributed to writing the paper.

COMPETING FINANCIAL INTERESTS

The authors declare no competing financial interests.

1. Roxburgh, S.A. *et al.* Allelic depletion of grem1 attenuates diabetic kidney disease. *Diabetes* **58**, 1641–1650 (2009).
2. Rodgers, J.T. *et al.* Nutrient control of glucose homeostasis through a complex of PGC-1α and SIRT1. *Nature* **434**, 113–118 (2005).
3. Bordone, L. & Guarente, L. Calorie restriction, SIRT1 and metabolism: understanding longevity. *Nat. Rev. Mol. Cell Biol.* **6**, 298–305 (2005).
4. Purushotham, A. *et al.* Hepatocyte-specific deletion of SIRT1 alters fatty acid metabolism and results in hepatic steatosis and inflammation. *Cell Metab.* **9**, 327–338 (2009).
5. Wang, R.H. *et al.* Hepatic Sirt1 deficiency in mice impairs mTorc2/Akt signaling and results in hyperglycemia, oxidative damage, and insulin resistance. *J. Clin. Invest.* **121**, 4477–4490 (2011).
6. Moynihan, K.A. *et al.* Increased dosage of mammalian Sir2 in pancreatic beta cells enhances glucose-stimulated insulin secretion in mice. *Cell Metab.* **2**, 105–117 (2005).
7. Kume, S. *et al.* Calorie restriction enhances cell adaptation to hypoxia through Sirt1-dependent mitochondrial autophagy in mouse aged kidney. *J. Clin. Invest.* **120**, 1043–1055 (2010).
8. He, W. *et al.* Sirt1 activation protects the mouse renal medulla from oxidative injury. *J. Clin. Invest.* **120**, 1056–1068 (2010).
9. Kitada, M., Kume, S., Imaizumi, N. & Koya, D. Resveratrol improves oxidative stress and protects against diabetic nephropathy through normalization of Mn-SOD dysfunction in AMPK/SIRT1-independent pathway. *Diabetes* **60**, 634–643 (2011).
10. Tikoo, K., Singh, K., Kabra, D., Sharma, V. & Gaikwad, A. Change in histone H3 phosphorylation, MAP kinase p38, SIR 2 and p53 expression by resveratrol in preventing streptozotocin induced type I diabetic nephropathy. *Free Radic. Res.* **42**, 397–404 (2008).
11. Kitada, M. *et al.* Dietary restriction ameliorates diabetic nephropathy through anti-inflammatory effects and regulation of the autophagy via restoration of Sirt1 in diabetic Wistar fatty (fa/fa) rats: a model of type 2 diabetes. *Exp. Diabetes Res.* **2011**, 908185 (2011).
12. Xu, Y. *et al.* Resveratrol protects against hyperglycemia-induced oxidative damage to mitochondria by activating SIRT1 in rat mesangial cells. *Toxicol. Appl. Pharmacol.* **259**, 395–401 (2012).
13. Hasegawa, K. *et al.* Sirt1 protects against oxidative stress–induced renal tubular cell apoptosis by the bidirectional regulation of catalase expression. *Biochem. Biophys. Res. Commun.* **372**, 51–56 (2008).
14. Hasegawa, K. *et al.* Kidney-specific overexpression of Sirt1 protects against acute kidney injury by retaining peroxisome function. *J. Biol. Chem.* **285**, 13045–13056 (2010).
15. Gilbert, R.E. & Cooper, M.E. The tubulointerstitium in progressive diabetic kidney disease: more than an aftermath of glomerular injury? *Kidney Int.* **56**, 1627–1637 (1999).
16. Nedachi, T., Kadotani, A., Ariga, M., Katagiri, H. & Kanzaki, M. Ambient glucose levels qualify the potency of insulin myogenic actions by regulating SIRT1 and FoxO3a in C2C12 myocytes. *Am. J. Physiol. Endocrinol. Metab.* **294**, E668–E678 (2008).
17. Orimo, M. *et al.* Protective role of SIRT1 in diabetic vascular dysfunction. *Arterioscler. Thromb. Vasc. Biol.* **29**, 889–894 (2009).
18. Gibb, D.M. *et al.* Renal tubular proteinuria and microalbuminuria in diabetic patients. *Arch. Dis. Child.* **64**, 129–134 (1989).
19. Vaidya, V.S. *et al.* Regression of microalbuminuria in type 1 diabetes is associated with lower levels of urinary tubular injury biomarkers, kidney injury molecule-1, and N-acetyl-β-D-glucosaminidase. *Kidney Int.* **79**, 464–470 (2011).
20. Bonventre, J.V. Can we target tubular damage to prevent renal function decline in diabetes? *Semin. Nephrol.* **32**, 452–462 (2012).
21. Ohse, T. *et al. De novo* expression of podocyte proteins in parietal epithelial cells during experimental glomerular disease. *Am. J. Physiol. Renal Physiol.* **298**, F702–F711 (2010).
22. Zhang, J. *et al. De novo* expression of podocyte proteins in parietal epithelial cells in experimental aging nephropathy. *Am. J. Physiol. Renal Physiol.* **302**, F571–F580 (2012).
23. Huby, A.C. *et al.* Restoration of podocyte structure and improvement of chronic renal disease in transgenic mice overexpressing renin. *PLoS ONE* **4**, e6721 (2009).
24. Ohse, T. *et al.* A new function for parietal epithelial cells: a second glomerular barrier. *Am. J. Physiol. Renal Physiol.* **297**, F1566–F1574 (2009).
25. Rincon-Choles, H. *et al.* ZO-1 expression and phosphorylation in diabetic nephropathy. *Diabetes* **55**, 894–900 (2006).
26. Zhang, Y. *et al.* Therapeutic approach for diabetic nephropathy using gene delivery of translocase of inner mitochondrial membrane 44 by reducing mitochondrial superoxide production. *J. Am. Soc. Nephrol.* **17**, 1090–1101 (2006).
27. Dai, C. *et al.* Wnt/β-catenin signaling promotes podocyte dysfunction and albuminuria. *J. Am. Soc. Nephrol.* **20**, 1997–2008 (2009).
28. Dhawan, P. *et al.* Claudin-1 regulates cellular transformation and metastatic behavior in colon cancer. *J. Clin. Invest.* **115**, 1765–1776 (2005).
29. Leelahavanichkul, A. *et al.* Angiotensin II overcomes strain-dependent resistance of rapid CKD progression in a new remnant kidney mouse model. *Kidney Int.* **78**, 1136–1153 (2010).
30. Boireau, S. *et al.* DNA-methylation–dependent alterations of Claudin-4 expression in human bladder carcinoma. *Carcinogenesis* **28**, 246–258 (2007).
31. Turek-Plewa, J. & Jagodziński, P.P. The role of mammalian DNA methyltransferases in the regulation of gene expression. *Cell Mol. Biol. Lett.* **10**, 631–647 (2005).
32. Fuks, F. DNA methylation and histone modifications: teaming up to silence genes. *Curr. Opin. Genet. Dev.* **15**, 490–495 (2005).
33. Peng, L. *et al.* SIRT1 deacetylates the DNA methyltransferase 1 (DNMT1) protein and alters its activities. *Mol. Cell. Biol.* **31**, 4720–4734 (2011).
34. O'Hagan, H.M., Mohammad, H.P. & Baylin, S.B. Double strand breaks can initiate gene silencing and SIRT1-dependent onset of DNA methylation in an exogenous promoter CpG island. *PLoS Genet.* **4**, e1000155 (2008).
35. Zhang, Q. *et al.* Metabolic regulation of SIRT1 transcription via a HIC1:CtBP corepressor complex. *Proc. Natl. Acad. Sci. USA* **104**, 829–833 (2007).
36. Wang, P. *et al.* Nicotinamide phosphoribosyltransferase protects against ischemic stroke through SIRT1-dependent adenosine monophosphate-activated kinase pathway. *Ann. Neurol.* **69**, 360–374 (2011).
37. Ramsey, K.M. *et al.* Age-associated loss of Sirt1-mediated enhancement of glucose-stimulated insulin secretion in beta cell–specific Sirt1-overexpressing (BESTO) mice. *Aging Cell* **7**, 78–88 (2008).
38. Wang, P. *et al.* Perivascular adipose tissue–derived visfatin is a vascular smooth muscle cell growth factor: role of nicotinamide mononucleotide. *Cardiovasc. Res.* **81**, 370–380 (2009).
39. Formentini, L., Moroni, F. & Chiarugi, A. Detection and pharmacological modulation of nicotinamide mononucleotide (NMN) *in vitro* and *in vivo*. *Biochem. Pharmacol.* **77**, 1612–1620 (2009).
40. Taha, H.M. *et al.* Molecular analysis of the interaction of anthrax adenylyl cyclase toxin, edema factor, with 2′(3′)-O-(N-(methyl)anthraniloyl)–substituted purine and pyrimidine nucleotides. *Mol. Pharmacol.* **75**, 693–703 (2009).
41. Lai, L.W., Moeckel, G.W. & Lien, Y.H. Kidney-targeted liposome-mediated gene transfer in mice. *Gene Ther.* **4**, 426–431 (1997).
42. Zhang, Z. *et al.* Regulated ATP release from astrocytes through lysosome exocytosis. *Nat. Cell Biol.* **9**, 945–953 (2007).
43. Peng, L. *et al.* Sirt1 deacetylates the DNA methyltransferase 1 (Dnmt1) protein and alters its activities. *Mol. Cell Biol.* **31**, 4720–4734 (2011).
44. Zorzano, A., Zorzano, A., Hernández-Alvarez, M.I., Palacín, M. & Mingrone, G. Alterations in the mitochondrial regulatory pathways constituted by the nuclear co-factors PGC-1α or PGC-1β and mitofusin 2 in skeletal muscle in type 2 diabetes. *Biochim. Biophys. Acta* **1797**, 1028–1033 (2010).
45. Nakahata, Y., Sahar, S., Astarita, G., Kaluzova, M. & Sassone-Corsi, P. Circadian control of the NAD+ salvage pathway by CLOCK-SIRT1. *Science* **324**, 654–657 (2009).

ONLINE METHODS

Production of TG and CKO mice. To prepare renal tubule–specific *SIRT1* TG mice on a C57BL/6J background, a transgenic expression vector containing a mouse *Npt2* (sodium phosphate cotransporter IIa) promoter and human *SIRT1* cDNA tagged with an eight-amino-acid Flag epitope was constructed as described previously[14]. Immunostaining using an antibody to Flag showed expression of the transgene in PTs but not glomeruli (**Supplementary Fig. 1c**). Mice were propagated as heterozygous TG mice by breeding them with WT C57BL/6 mice. F2 mice were used as TG mice, and age- and sex-matched littermates were used as WT control mice. Kidney-specific *Sirt1* knockout ($Sirt1^{-/-}$) mice (CKO mice) were produced by crossing $Sirt1^{flox/flox}$ mice on a C57BL/6J background with γ-GT–Cre mice (Jackson Laboratory)[46]. γ-GT–Cre TG mice on a C57BL/6J background have demonstrated PT-specific Cre recombinase activity[2]. Therefore, $Sirt1^{flox/flox}$ γ-GT–$Cre^{TG/+}$ (PT-specific $Sirt1^{-/-}$) mice had a specific deletion of *Sirt1* in PTs. The following three types of control mice were produced by this breeding: $Sirt1^{flox/flox}$, $Sirt1^{+/+}$ γ-GT–$Cre^{TG/+}$ and $Sirt1^{+/+}$. In the following studies, $Sirt1^{flox/flox}$ γ-GT–$Cre^{TG/+}$ mice were crossed with $Sirt1^{flox/flox}$ mice to produce $Sirt1^{flox/flox}$ γ-GT–$Cre^{TG/+}$ (PT-specific $Sirt1^{-/-}$) mice. $Sirt1^{flox/flox}$ mice were used as control mice. All animal studies were performed in accordance with the animal experimentation guidelines of Keio University School of Medicine.

Podocyte-specific Claudin-1 overexpression in mice. Mouse *Cldn1* cDNA was cloned as described previously[47]. The cDNA was inserted downstream of a podocyte-specific promoter, a 2.5-kb fragment of the human *NPHS2* (podocin) promoter[48]. Eight-week-old male mice were treated with saline or STZ. One week after saline or STZ injection, 50 μg of 2.5 AU hemagglutination virus of Japan (HVJ) envelope vector (GenomeONE-Neo, Ishihara Sangyo, Osaka, Japan) that carried plasmid DNA was injected into the tail vein in 120 μl of suspension buffer weekly. Mice were killed 24 weeks after injection.

Experimental protocol for animal experiments. *STZ treatment.* Eight-week-old male mice were treated with STZ (Sigma-Aldrich, St. Louis, MO) dissolved in 100 mmol l^{-1} citrate buffer, pH 4.5, or with PBS dissolved in citrate buffer.

db/db mice. To produce compound-mutant mice with a *SIRT1* TG *db/db* genotype, PT-specific *SIRT1* TG mice were bred with male mice heterozygous for the *db* mutation (*db/m*). Both the *SIRT1* TG and *db* heterozygous breeders were on a C57BL/6J genetic background. Offspring from the F1 generation, which were heterozygous for the *db* mutation and also expressed the *SIRT1* transgene, were then bred with mice heterozygous for the *db* mutation. The F2 generation contained the desired compound mutant (*SIRT1* TG *db/db*), plus the other genotypes used. The following four genotypes were used: WT nontransgenic ND, WT *db/db*, TG ND and TG *db/db*. At the age of 6 months, mice were euthanized.

5/6Nx. Eight-week-old male C57BL/6 mice were subjected to 5/6Nx in two stages[29]. In the first stage, the left kidney was decapsulated, and then the upper and lower poles were partially resected through a left flank incision during the second stage. After 1 week, the entire right kidney was removed[5]. Sham-operated mice were used as controls. Twenty-four weeks after surgery, kidney tissues were harvested.

FK866 treatment. FK866 (Sigma, St. Louis, MO) was dissolved in DMSO, and 25 mg ml^{-1} aliquots were stored at −80 °C until further use. Male C57BL/6 mice received intraperitoneal injections of 30 mg per kg body weight FK866 further diluted in PBS twice a day 3 d a week from 8 weeks to 32 weeks of age.

Histopathological examination. PAS-stained samples from 30 consecutive glomeruli per animal were examined. The glomerular area was traced along the outline of the capillary loop using Image-Pro Plus 3.0 (Media Cybernetics, Silver Spring, MD). The extent of the mesangial matrix was determined by assessment of the PAS-positive and nucleus-free areas in the mesangium. Immunohistochemistry was performed as previously described[14]. Briefly, paraffin sections (4 μm) were fixed in 3% formaldehyde and stained using primary antibodies to Flag (Sigma, F 1804, 1:250), Sirt1 (Millipore, Bedford, MA, 07-131, 1:200) and Claudin-1 (Invitrogen, San Diego, CA, 51-9000, 1:50). The sections were stained with biotin-labeled goat antibody to rabbit IgG (Vector, BA-1000, 1:200) or biotin-labeled antibody to mouse IgG (Vector, BA-9200, 1:200) and then treated with the Vectastain Elite ABC Kit (Vector).

Immunofluorescence staining. Indirect immunofluorescence staining for Sirt1 was carried out on frozen kidney sections using rabbit monoclonal antibody to Sirt1 (Cell Signaling Technology, 9475, 1:200). Alexa Fluor goat antibody to rabbit IgG (Molecular Probes, Eugene, OR, USA, A-11008, 1:200) was used as the secondary antibody. As a negative control, the primary antibody was replaced with nonimmune serum from the same species; no staining occurred. Immunofluorescence staining for AQP-1 (Santa Cruz, sc-252871, 1:100) was performed in a similar manner using respective antibodies. For fluorescence microscopy, all sections were stained and analyzed at the same time to exclude artifacts due to variable decay of the fluorochrome. Sections were examined using a Nikon Microphot-FX fluorescence microscope equipped with a Spot II digital camera.

EM. For EM evaluation, kidney tissue was embedded in Epon epoxy resin (Miller-Stephenson Chemical Company, Sylmar, CA)[49]. Electron micrographs of ten glomeruli per kidney were taken randomly for each mouse to evaluate podocyte morphometry. Photomicrographs of the GBM were analyzed for the density of tight-slit pores between the podocyte foot processes according to published methods[6]. Tight-slit pores were identified by the obliteration of spaces between adjacent foot processes. The numbers of tight-slit pores were counted and divided by the GBM length (mm) to determine the density of tight-slit pores. A total of 500 foot processes from each group were evaluated for the analysis of slit pore density.

Immunogold EM. Mouse kidneys from the four groups were finely chopped, fixed in 4% paraformaldehyde and 0.2% picric acid and embedded in LR white resin (London Resin, Basingstoke, UK). Ultrathin sections were blocked with goat IgG and incubated with rabbit antibody to Claudin-1 (Invitrogen, 51-9000, 1:50) followed by 15 nm colloidal gold-conjugated goat antibody to rabbit IgG (EBS, East Granby, CT, BC-GAR, 1:100). Grids were counterstained with 0.5% osmium and 1% uranyl acetate, and bound gold particles were visualized and photographed by EM. The numbers of gold particles per μm^2 were then counted using Scion software, and the averages were compared statistically.

Laser microdissection. Laser microdissection was performed according to previous reports[50,51]. We used poly-L-lysine to prevent PECs (kindly provided by S.J. Shankland and C. Campbell, Division of Nephrology, University of Washington) from detaching from glass slides and a modified PAS staining protocol specific for laser microdissection samples from cryosections that is not generally used on paraffin-embedded samples. Freshly frozen kidney tissue was cut into 7-μm-thick sections. Cryosections were mounted onto a polyethylene membrane that was previously attached to a glass slide that had been coated with 0.1% poly-L-lysine (Sigma-Aldrich). The sections were stained with PAS, counterstained with haematoxylin and stored at −80 °C until use. These tissues were excised using a PALM MicroBeam IP 230V Z microscope for laser pressure catapulting (P.A.L.M. Microlaser Technologies, Bernried, Germany) as described previously[51]. RNA from microdissected tissue was prepared using the PALM RNA extraction kit.

Microarray analysis. Mice in the STZ-treated WT and TG groups were killed at 32 weeks of age. Before microarray analysis, we dissected the glomerular regions. Microdissected glomeruli were immediately used for total RNA isolation and subjected to analysis on Affymetrix Mouse Genome 430 2.0 microarray chips according to Affymetrix standard protocols (http://www.affymetrix.com). Genes were excluded if the signal strength did not significantly exceed the background values and if the expression did not reach a threshold value for reliable detection ($P < 0.05$) in each of the three separate studies. Genes were also excluded if the level of expression did not vary by more than fourfold or less than 0.25-fold between the STZ-treated WT and TG groups. The remaining genes were subjected to nonparametric Welch *t* tests and are reported with their respective fold changes and *P* values.

Culture of podocytes and HK-2 cells. Conditionally immortalized mouse podocytes were donated by P. Mundel (Mt. Sinai School of Medicine, New York, NY, USA) and K. Asanuma (Juntendo University, Tokyo, Japan)[52]. Mouse *Cldn1* cDNA was cloned as described previously[47]. In CM experiments, control

vector– or *SIRT1* vector–transfected HK-2 cells seeded at a density of 5×10^5 per 100 mm^2 were cultured for 24 h with either NG (5 mM) or HG (25 mM). The CM from each treatment was then transferred onto culture plates containing podocytes. DMEM containing 10% FBS was used for both cell types. Podocytes were seeded at a density of 5×10^5 per 100 mm^2, incubated for 7 d (differentiation) and used for experiments. Differentiation of cells was confirmed as previously described[52]. The NAD^+-to-NADH ratio was measured in whole-cell extracts of HK-2 cells or podocytes using the BioVision NAD^+/NADH Quantitation Kit (BioVision, Mountain View, CA). NMN was detected by HPLC as previously described[39].

Culture of HRE cells. Primary HRE cells (Clonetics, San Diego, CA) were cultured according to the manufacturer's instructions. The expression plasmid containing human *SIRT1* cDNA (pcDNA3.1-*SIRT1*) and the control plasmid (pcDNA3.1) were transfected into HRE cells using Lipofectamine 2000 (Invitrogen). For treatment with 5-aza-dC (Sigma-Aldrich), the cells were treated with 5 μM 5-aza-dC for 96 h. For *Dnmt* siRNA treatment, a *Dnmt* siRNA duplex was purchased from Sigma-Aldrich. The sense sequences were 5′-[dT] GGAAUGGCAGAUGCCAACAGC [dT]-3′ for Dnmt1, 5′-[dT] GAA AGCGAAGGUCAUUGCA [dT]-3′ for Dnmt3a and 5′-[dT] GCUAGCGA AGGUCAUUGCA [dT]-3′ for Dnmt3b. Control siRNA consisted of a scrambled siRNA construct encoding a nonspecific siRNA without mammalian homology. These siRNAs (100 pmol μl^{-1}) were transfected using Lipofectamine 2000 (Invitrogen) for 24 h.

RNA isolation, reverse transcription and quantitative PCR. Real-time PCR was performed using the ABI Prism 7700 sequence detection system (Applied Biosystems, Foster City, CA) and the SYBR GREEN system (Applied Biosystems)[13,14]. The sequences of the primers used are listed in **Supplementary Tables 4** and **5**. The relative mRNA levels for the specific genes were normalized to the level of mRNA expression for the housekeeping gene *Gapdh*.

Immunoblotting. Immunoblotting was performed as described previously[13,14] using specific antibodies to Sirt1 (Millipore, 07-131, 1:1,000) and Claudin-1 (Invitrogen, 51-9000, 1:100). For assaying β-catenin–Snail signaling, a primary antibody to synaptopodin (Sigma, St. Louis, MO; Biodesign, Sabo, ME, G1D4, undiluted), an antibody to β-catenin (BD Transduction Laboratories, San Jose, CA, 610154, 1:1,000) and an antibody to Snail (Abcam, ab17732, 1:200) were used. The β-actin band recognized by a specific antibody (Sigma, AC-15, 1:10,000) was used as a loading control. Band intensities were quantified using Scion Image Software (Scion Corp, Frederick, MD).

Claudin-1 CpG methylation *in vivo* by methylation-specific PCR (MSP) and real-time MSP. Total genomic DNA from the kidneys or HRE cells was extracted using a DNeasy Kit (Qiagen Japan, Tokyo). Bisulfite conversion of genomic DNA was performed using a Zymo EZ DNA Methylation Gold kit (Zymo Research Corp., Orange, CA). MSP was performed to determine the methylation status of the *Cldn1* gene, and real-time MSP was performed for quantitative analysis of the methylation of the *Cldn1* gene as described previously[11]. Specific methylated or unmethylated sequences of the primer sets used are listed in **Supplementary Table 6**. Two independent bisulfite modifications were performed, and five independent MSPs and real-time MSPs were performed. Representative bands of MSP are shown in the figures[53].

Bisulfite genomic sequencing. DNA was extracted from cells according to standard procedures. A 2-μg quantity of DNA was then treated with bisulfite using the EpiTect Bisulfite Kit (Qiagen) and amplified by nested PCR using the following PCR primers: PCR1 forward: 5′-AGTTGTATAGAGAGTAA GGGTATAGGT-3′, reverse: 5′-TTAACCTAAAACTTAAATTCTTTCTAC-3′; PCR2 forward: 5′-AGGTATTAATT TGTTTGTAGAGATT-3′, reverse: 5′-TAACCTCTAAACTAAATAAAACTACTACA-3′. PCR products were cloned using the TOPO TA cloning kit (Invitrogen). Ten random clones were sequenced using an ABI3730 DNA analyzer (Applied Biosystems) with the following sequence primers: forward: 5′-CAGGAAACAGCTATGAC-3′, reverse: 5′-GTTTTCCCAGTCACGACGT-3′.

***SIRT1* siRNA experiments.** The siRNA for *SIRT1* was prepared by Japan Bio Service (JBios, Saitama, Japan). The targeted sequence to silence the transcription of *SIRT1* was 5′-GAAGTTGACCTCCTCATTG-3′. An siRNA targeting sequence for GFP (5′-GGCTACGTCCAGCAGCGCACC-3′) mRNA was used as a negative control. As another negative control, a scrambled siRNA (JBioS) that did not exhibit homology to any coding region was used. The sequence 5′-TCCGAACGTGGCACGA-3′ was used as the scrambled siRNA control.

ChIP assay. HRE cells were treated with or without the Sirt1 inhibitor sirtinol (20 μM; Sigma-Aldrich) for 48 h and used for the following ChIP assay. The ChIP assay was performed with 1×10^6 HRE cells per assay using the ChIP assay kit (Upstate Biotechnology Inc., Lake Placid, NY) as described by the manufacturer's protocol. All antibodies used in this study were purchased from Abcam. Antibodies against H3ac (ab47915, 1:20,000), H4ac (ab46983, 1:20,000), H3K9me2 (ab1220, 1:5,000), H3K27me2 (ab24684, 1:5,000) and H4K20me2 (ab9052, 1:5,000) were used for immunoprecipitation (IP), and rabbit IgG was used as a negative control to check the specificity of IP. After IP, recovered chromatin samples were subjected to PCR with the following set of primers: AACTCTCCGCCTTCTGCAC and ACACGCAGGACATCCACAG for the CpG region of *Cldn1* and CCGTTGGCATGAAGTGTATG and AAGGCAGAGAGAAGCAGCAG for the non-CpG region of *Cldn1*. The PCR products were run on agarose gels. The results from three independent experiments are presented.

Quantification of NMN autofluorescence by photoactivatable NMN. Intracellular endogenous NMN autofluorescence was monitored by confocal microscopy as described previously[39] with slight modification. Briefly, 100 ml of 1 N $HClO_4$ was added to cells or kidney sections on a culture dish or glass plate. Then these sections were embedded with 1 N KOH, and after 5 min an additional 100 ml of 0.1 M bicine, pH 7.4, was added, followed by 1 N KOH and acetophenone. These samples were incubated for 15 min, and then 100 ml formic acid was added. By means of this derivatization procedure, NMN shows fluorescence with peaks of excitation and emission in the regions of 332 nm and 454 nm, respectively. A confocal microscope equipped with a custom 340 ± 10 nm excitation and 460 ± 25 nm emission filter set was used together with a Zeiss Axiocam digital camera (Carl Zeiss) for imaging intrinsic NMN autofluorescence from HK-2 cells, podocytes or kidney sections freshly isolated from each mouse. Collected images were subsequently analyzed using Zeiss Axiovision 4.4 software. Background fluorescence intensity was subtracted from each data point.

Synthesis of Mant-NMN and intrarenal artery injection of Mant-NMN. To elucidate whether NMN is released from PTs and then mobilized into podocytes, fluorescence-labeled exogenous NMN was injected into mice. We used Mant for labeling NMN. Mant-NMN was synthesized as described[39,40]. Saline or Mant-NMN (500 mg per kg body weight) was administered by intra-arterial injection into 8-week-old male mice as described[41]. Thereafter, kidney samples were harvested 1, 2 and 4 h after NMN injection, and tissues were examined by confocal microscopy using an LSM 510 Zeiss microscope. Fluorescence was detected at 430–480 nm, with excitation at 364 nm to detect the signal of Mant. To confirm whether positive signals of Mant-NMN conformed with PTs or podocytes, sequential sections were used for immunofluorescence staining of kidney sections. The primary antibodies used for immunofluorescence studies were to AQP-1 (a PT marker) (Santa Cruz Biotechnology, sc-252871, 1:1,000) and podocin (a podocyte marker) (Sigma-Aldrich, P0732, 1:100).

Human renal specimens from needle biopsy. Needle renal biopsy specimens were obtained from 11 subjects with diabetic nephropathy. No subjects received steroids or immunosuppressive drugs before renal biopsy. As controls, pretransplant biopsies from five living donors were obtained. Clinical data from the subjects were documented at the time of renal biopsy and are summarized in **Supplementary Table 3**. The value of eGFR was calculated with a revised modification of diet in renal disease (MDRD) equation for the Japanese population: eGFR (ml min^{-1} 1.73 m^{-2}). Human kidney samples were collected from renal biopsies at the Japanese Red Cross Shizuoka Hospital. Written informed consent was obtained from all participants. The study was performed in accordance with the declaration of Helsinki, and the study protocol was approved by the Human Ethics Review Committee of the Japanese Red Cross Shizuoka Hospital. Immunohistochemistry for SIRT1 or Claudin-1 was performed on each human

doi:10.1038/nm.3363

sample essentially as described previously. Results are reported as the labeling index, which represents the percentage of total glomerular tuft area that was stained.

Statistical analyses. Data are expressed as the means ± s.e.m. Data were analyzed using one- or two-way analysis of variance, as appropriate, followed by Bonferroni's multiple comparison *post hoc* test. $P < 0.05$ was considered statistically significant.

46. Clodfelder-Miller, B., Sarno, P.D., Zmijewska, A.A., Song, L. & Jope, R.S. Physiological and pathological changes in glucose regulate brain Akt and glycogen synthase kinase-3. *J. Biol. Chem.* **280**, 39723–39731 (2005).
47. Leotlela, P.D. *et al.* Claudin-1 overexpression in melanoma is regulated by PKC and contributes to melanoma cell motility. *Oncogene* **26**, 3846–3856 (2007).
48. Moeller, M.J., Sanden, S.K., Soofi, A., Wiggins, R.C. & Holzman, L.B. Podocyte-specific expression of cre recombinase in transgenic mice. *Genesis* **35**, 39–42 (2003).
49. Sung, S.H. *et al.* Blockade of vascular endothelial growth factor signaling ameliorates diabetic albuminuria in mice. *J. Am. Soc. Nephrol.* **17**, 3093–3104 (2006).
50. Cohen, C.D. *et al.* Laser microdissection and gene expression analysis on formaldehyde-fixed archival tissue. *Kidney Int.* **61**, 125–132 (2002).
51. Kohda, Y. *et al.* Analysis of segmental renal gene expression by laser capture microdissection. *Kidney Int.* **57**, 321–331 (2000).
52. Asanuma, K., Campbell, K.N., Kim, K., Faul, C. & Mundel, P. Nuclear relocation of the nephrin and CD2AP-binding protein dendrin promotes apoptosis of podocytes. *Proc. Natl. Acad. Sci. USA* **104**, 10134–10139 (2007).
53. Terasawa, K. *et al.* Epigenetic inactivation of TMS1/ASC in ovarian cancer. *Clin. Cancer Res.* **10**, 2000–2006 (2004).

OPEN ACCESS Freely available online

PLOS ONE

C-Reactive Protein, High-Molecular-Weight Adiponectin and Development of Metabolic Syndrome in the Japanese General Population: A Longitudinal Cohort Study

Yoshifumi Saisho[1]*, Hiroshi Hirose[2], Rachel Roberts[3], Takayuki Abe[3], Hiroshi Kawabe[2], Hiroshi Itoh[1]

1 Department of Internal Medicine, Keio University School of Medicine, Tokyo, Japan, **2** Health Center, Keio University School of Medicine, Tokyo, Japan, **3** Center for Clinical Research, Keio University School of Medicine, Tokyo, Japan

Abstract

Aims: To clarify predictive values of C-reactive protein (CRP) and high-molecular-weight (HMW) adiponectin for development of metabolic syndrome.

Research Design and Methods: We conducted a prospective cohort study of Japanese workers who had participated in an annual health checkup in 2007 and 2011. A total of 750 subjects (558 men and 192 women, age 46±8 years) who had not met the criteria of metabolic syndrome and whose CRP and HMW-adiponectin levels had been measured in 2007 were enrolled in this study. Associations between CRP, HMW-adiponectin and development of metabolic syndrome after 4 years were assessed by logistic regression analysis and their predictive values were compared by receiver operating characteristic analysis.

Results: Among 750 subjects, 61 (8.1%) developed metabolic syndrome defined by modified National Cholesterol Education Program Adult Treatment Panel III (NCEP-ATP III) criteria and 53 (7.1%) developed metabolic syndrome defined by Japan Society for the Study of Obesity (JASSO) in 2011. Although CRP and HMW-adiponectin were both significantly correlated with development of metabolic syndrome, multivariate logistic regression analysis revealed that HMW-adiponectin but not CRP was associated with metabolic syndrome independently of BMI or waist circumference. Adding these biomarkers to BMI or waist circumference did not improve the predictive value for metabolic syndrome.

Conclusion: Our findings indicate that the traditional markers of adiposity such as BMI or waist circumference remain superior markers for predicting metabolic syndrome compared to CRP, HMW-adiponectin, or the combination of both among the Japanese population.

Citation: Saisho Y, Hirose H, Roberts R, Abe T, Kawabe H, et al. (2013) C-Reactive Protein, High-Molecular-Weight Adiponectin and Development of Metabolic Syndrome in the Japanese General Population: A Longitudinal Cohort Study. PLoS ONE 8(9): e73430. doi:10.1371/journal.pone.0073430

Editor: Hideharu Abe, University of Tokushima, Japan

Received March 8, 2013; **Accepted** July 22, 2013; **Published** September 12, 2013

Funding: This study was supported in part by a Grant-in Aid from the Ministry of Education, Culture, Sports, Science and Technology, Japan (to H.H.), and by research grants from Keio University, Tokyo (to H.H.). The funders had no role in study design, data collection and analysis, decision to publish, or preparation of the manuscript.

Competing Interests: Fujirebio Co., Tokyo and Keio University, Tokyo have a partial patent concerning HMW-adiponectin measurement kit ("Methods for diagnosis or monitoring of impaired glucose tolerance", WO2003/016906, JP-3624216 (2004) and JP-4214202 (2008)). This does not alter the authors' adherence to all the PLOS ONE policies on sharing data and materials.

* E-mail: ysaisho@z5.keio.jp

Introduction

Metabolic syndrome is now widely appreciated as a cluster of metabolic abnormalities such as visceral obesity, hypertension, hyperglycemia and dyslipidemia [1]. To date, incidence of metabolic syndrome is continuously increasing worldwide. Since subjects with metabolic syndrome are at risk for development of type 2 diabetes, cardiovascular disease (CVD) and cancer [1,2], prevention of metabolic syndrome is an urgent issue.

Higher levels of C-reactive protein (CRP) and lower levels of high-molecular-weight (HMW) adiponectin have been both reported to correlate with obesity and metabolic syndrome [3,4,5,6]. These biomarkers have been also reported to correlate with type 2 diabetes and CVD [5,7,8,9,10,11]. Therefore, these biomarkers appear to be useful to detect subjects at high risk of metabolic syndrome, type 2 diabetes and CVD.

Although associations between CRP or HMW-adiponectin and metabolic syndrome have been well established, there have been few studies to examine the usefulness of combination of both biomarkers for prediction of metabolic syndrome. Especially, in clinical settings it is essential to compare the predictive utility of these biomarkers for metabolic syndrome with that of the traditional markers. Therefore, in this longitudinal cohort study we sought to address the following questions: 1) Is there any additive effect of the combination of CRP and HMW-adiponectin for prediction of metabolic syndrome compared with each of them

alone? 2) Are predictive values of the traditional markers such as BMI or waist circumference for metabolic syndrome improved by adding these biomarkers?

Methods

Ethics Statement

The present study was conducted according to the principles expressed in the Declaration of Helsinki. Written informed consent was obtained from each subject after a full explanation of the purpose, nature and risk of all procedures used. The protocol was approved by the ethical review committees of the Health Center and the Faculty of Medicine, Keio University School of Medicine, Tokyo, Japan.

Subjects

We conducted a prospective cohort study of 1,552 Japanese teachers and workers at Keio University (1,067 men and 485 women) who had participated in an annual health checkup in 2007. More than 95% of the workers and teachers at Keio University participated in this annual health checkup. In this study, we primarily enrolled subjects aged 40 years and older because the incidence of metabolic syndrome is low in the subjects younger than 40 years old [12]. Then we randomly enrolled subjects younger than 40 years old. As a result, we measured CRP and HMW-adiponectin in 1,250 subjects out of 1,552 subjects (81%). Among them, 42 subjects were excluded because of their CRP>0.5 mg/L. Of those (1,208 subjects), 884 subjects (73%, 676 men and 208 women) had been followed up in an annual health checkup in 2011. Finally, a total of 750 subjects (558 men and 192 women, age 46±8 years) who had not met the criteria of metabolic syndrome defined by National Cholesterol Education Program Adult Treatment Panel III (NCEP-ATP III) and Japan Society for the Study of Obesity (JASSO) in 2007 were enrolled in this study (Table 1). The subjects with whom we were not able to follow up in 2011 (N = 324) were older (49±14 vs. 47±8 years, $p<0.05$) and predominantly female (32.4% vs. 23.5%, $p<0.05$) than the study participants (N = 884), although the difference was clinically small, presumably reflecting retirement or resignation from work. Information regarding smoking, alcohol intake, physical activity and medication was obtained from questionnaires to the subjects.

Measurement

Systolic and diastolic blood pressure was measured in the sitting position after resting for at least 3 min using an automatic electronic sphygmomanometer (BP-103i II; Nippon Colin, Komaki, Japan) with cuff size of 14.5 cm in width and 52.0 cm in length. Blood samples were collected in the morning after an overnight fast.

Plasma glucose and serum lipids were assayed by routine automated laboratory methods as previously described [13]. Serum insulin concentration was measured by an enzyme immunoassay, using a commercially available kit (Tosoh, Tokyo, Japan), with intra- and interassay coefficients of 2.9 to 4.6% and 4.5 to 7.0%, respectively. The insulin resistance index was assessed by a homeostasis model assessment of insulin resistance (HOMA-IR), which was calculated as fasting serum insulin (mU/L) × fasting plasma glucose (mmol/L)/22.5 [14].

HMW-adiponectin was measured using a commercially available kit (HMW adiponectin ELISA Kit, Fujirebio, Tokyo, Japan) as previously reported [13]. This ELISA system does not need a denaturing step, and the monoclonal antibody (IH7) is reported to react specifically with the HMW form of adiponectin [15]. The dilution curve was parallel to the standard curve. Intra- and interassay coefficients were 2.4 to 3.0% and 4.2 to 5.1%, respectively. We have previously reported that HMW-adiponectin and HMW-adioponectin to total adiponectin ratio were more sensitively associated with metabolic syndrome than total adiponectin alone [16,17,18]. Thus we measured HMW-adiponectin rather than total adiponectin in this study. Serum CRP levels were measured by nephelometry, a latex particle-enhanced immunoassay (N Latex CRP II, Dade Behring, Tokyo, Japan) with both intra- and interassay coefficients of <5.0%. For the analysis of CRP values under the assay detection limit of 0.04 mg/L, an approximate value of 0.02 mg/L was used.

Definition of Metabolic Syndrome

Metabolic syndrome (MetS) was defined according to the revised NCEP ATP III criteria [1] as 3 or more of 5 components in which the cut-off point of waist circumference was modified for Japanese as ≥90 cm in men and ≥80 cm in women according to the recommendation by the International Diabetes Federation (IDF) [19], the cut-off points of the other components were systolic blood pressure ≥130 mmHg and/or diastolic blood pressure ≥85 mmHg for blood pressure, ≥150 mg/dL for triglycerides, <40 mg/dL in men and <50 mg/dL in women for HDL-cholesterol, and ≥100 mg/dL for fasting plasma glucose. Subjects receiving antihypertensive, lipid-lowering agent or hypoglycemic medication were considered to have the respective component. Japanese metabolic syndrome (JMetS) defined by the Examination Committee for Criteria of Metabolic Syndrome [20] was also examined. The criteria of JMetS is waist circumference ≥85 cm in men and ≥90 cm in women plus 2 or more of the following 3 components; systolic blood pressure ≥130 mmHg and/or diastolic blood pressure ≥85 mmHg, triglycerides ≥150 mg/dL and/or HDL cholesterol <40 mg/dL, and fasting plasma glucose ≥110 mg/dL.

Statistical Analysis

Comparisons between the two groups were performed with Student's t-tests or Fisher's exact tests and odds ratios were determined by logistic regression analysis using the Statistical Package for the Social Sciences (version 19.0; SPSS, Chicago, IL, USA). Receiver operating characteristic (ROC) curves for MetS and JMetS were plotted separately and the area under the curve (AUC) (also referred to as C-statistic in the case of a binary outcome) of ROC curves was calculated. ROC analysis was performed using Proc Logistic in SAS 9.2 (SAS Institute, Cary, NC), which estimates AUC using the trapezoidal method of integration of the sensitivity curve. All normally distributed data are expressed as mean ± S.D., while non-normal data are expressed as median (interquartile range) and the logarithms of the non-normal data were used for the analyses. Values of $p<0.05$ were considered statistically significant.

Results

Baseline Characteristics of Subjects According to Development of Metabolic Syndrome

During 4 years, 61 subjects (8.1%, 51 men and 10 women) developed MetS and 53 (7.1%, 50 men and 3 women) developed JMetS, respectively. Comparisons of baseline characteristics according to the development of metabolic syndrome are shown in Table 1. CRP and C/A ratio were significantly higher, and HMW-adiponectin was significantly lower in subjects who developed metabolic syndrome compared with those who did not (all $p<0.001$). HMW-adiponectin and CRP are significantly

Table 1. Characteristics of subjects according to development of metabolic syndrome after 4 years.

	Total	MetS		JMetS	
		(−)	(+)	(−)	(+)
N	750	689	61	697	53
Male (%)	74.4	73.6	83.6	72.9	94.3†
Age (years)	46±8	46±8	49±8**	46±8	50±7†
Height (m)	1.68±0.08	1.68±0.08	1.69±0.08	1.68±0.08	1.69±0.06
Weight (kg)	63.4±15.5	62.7±10.5	71.2±10.6†	62.7±10.6	71.4±8.8†
BMI (kg/m^2)	22.4±2.9	22.2±2.7	24.9±3.0†	22.2±2.8	24.9±2.8†
Waist circumference (cm)	80.1±8.2	79.5±8.0	86.7±7.7†	79.6±8.0	87.5±6.6†
Systolic blood pressure (mmHg)	120±16	119±15	132±16†	119±15	132±14†
Diastolic blood pressure (mmHg)	75±11	75±11	84±11†	75±11	84±8†
Heart rate (bpm)	76±12	75±12	79±11*	75±12	79±11*
Current smoking (%)	8.9	9.1	6.6	8.8	11.3
Alcohol intake (≥20 g/day) (%)	21.3	20.6	29.5	19.8	41.5**
No exercise (<150 min/week) (%)	61.9	62.3	57.4	62.4	54.7
Antihypertensives (%)	6.4	4.8	24.6†	4.6	30.2†
Lipid-lowering agents (%)	1.7	1.2	8.2**	1.9	0.0
Oral hypoglycemic agents (%)	0.7	0.7	0.0	0.4	3.8*
AST (IU/L)	20 (17–24)	20 (17–24)	20 (17–25)	20 (17–23)	24 (19–28)**
ALT (IU/L)	20 (14–26)	19 (14–26)	24 (17–36)*	19 (14–26)	26 (20–36)**
γ-GTP (IU/L)	26 (17–42)	25 (17–40)	37 (26–71)*	24 (17–40)	47 (32–80)**
ALP (IU/L)	198±59	198±58	206±62	198±59	201±58
Glucose (mg/dL)	89 (85–94)	89 (85–94)	94 (89–97)*	89 (85–94)	94 (91–98)**
Total cholesterol (mg/dL)	206±30	205±29	216±35*	206±30	207±30
LDL-cholesterol (mg/dL)	121±28	120±27	135±35**	121±27	123±32
HDL-cholesterol (mg/dL)	64±16	64±16	56±12†	64±16	55±11†
Triglyceride (mg/dL)	79 (53–113)	76 (52–110)	114 (84–148)†	75 (52–109)	123 (97–149)†
Uric acid (mg/dL)	5.6±1.4	5.6±1.4	6.3±1.1†	5.6±1.3	6.6±1.2†
Creatinine (mg/dL)	0.78±0.14	0.78±0.14	0.81±0.16	0.78±0.14	0.84±0.13**
Insulin (mU/L)	4.1 (3.0–5.8)	4.1 (3.0–5.7)	5.2 (3.9–7.1)	4.1 (3–5.6)	5.8 (3.9–7.4)*
HOMA-IR	0.91 (0.67–1.31)	0.89 (0.66–1.27)	1.18 (0.86–1.68)*	0.89 (0.66–1.26)	1.40 (0.94–1.75)**
CRP (mg/L)	0.28 (0.13–0.62)	0.26 (0.12–0.60)	0.54 (0.23–0.78)†	0.26 (0.12–0.6)	0.54 (0.33–0.74)†
HMW-adiponectin (μg/mL)	4.0 (2.5–6.3)	4.2 (2.6–6.5)	2.7 (1.8–3.9)†	4.3 (2.6–6.5)	2.3 (1.6–3.3)†
C/A ratio	0.08 (0.03–0.19)	0.07 (0.02–0.18)	0.20 (0.08–0.41)†	0.07 (0.02–0.18)	0.24 (0.10–0.41)†

Values are expressed as mean ± SD for variables with normal distribution and median (interquartile range) for those with non-normal distribution. MetS; metabolic syndrome, JMetS; Japanese metabolic syndrome.
*P<0.05,
**P<0.01,
†P<0.001 vs. MetS(−) or JMetS(−).
doi:10.1371/journal.pone.0073430.t001

correlated with BMI and waist circumference (Table 2), whereas the correlation was stronger in HMW-adiponectin compared with CRP.

Association between CRP, HMW-adiponectin and Development of Metabolic Syndrome

In univariate logistic regression analysis, both CRP and HMW-adiponectin were significantly associated with development of metabolic syndrome (odds ratio: 1.54 and 0.45 for MetS and 1.65 and 0.33 for JMetS, respectively, Table 3). However, when the model was adjusted for age, sex and traditional markers of adiposity such as BMI or waist circumference, HMW-adiponectin, but not CRP, was significantly associated with development of metabolic syndrome (Table 3). Adding the other variables which relate to development of metabolic syndrome to the model did not change the results (Models 3 and 4, Table S1).

Predictive Values of CRP and HMW-adiponectin for Metabolic Syndrome

Finally we evaluated additive effects of CRP and HMW-adiponectin on BMI and waist circumference for prediction of metabolic syndrome (Table 4). ROC analysis revealed that there is no significant change in the AUC of the combination of CRP and HMW-adiponectin compared with that of each of them alone. The AUC of BMI or waist circumference itself was greater than that of CRP, HMW-adiponectin or the combination of both.

Table 2. Correlations among HMW-adiponectin, CRP, BMI and waist circumference.

	BMI	Waist circumference	HMW-adiponectin	CRP
BMI	1	0.853**	−0.413**	0.194**
Waist circumference	0.853**	1	−0.409**	0.221**
HMW-adiponectin	−0.413**	−0.409**	1	−0.117*
CRP	0.194**	0.221**	−0.117*	1

*P = 0.001,
**P<0.001.
doi:10.1371/journal.pone.0073430.t002

Comparison between predictive ability of the models using CRP and HMW-adiponectin after adjusting for BMI or waist circumference, and the models using BMI or waist circumference alone, was done using the ROCCONTRAST statement in SAS. All but one of these comparisons showed no significant difference, but the only significant difference was not meaningful, as the actual difference in AUC was less than 1%. Thus the AUC of BMI or waist circumference was not significantly improved by adding CRP, HMW-adiponectin or both. These findings did not change when the subjects were stratified by sex (Tables S2 and S3).

Discussion

In this study, we report that 1) Combination of CRP and HMW-adiponectin did not improve predictive value for metabolic syndrome compared with each of them alone, 2) Adding these biomarkers to BMI or waist circumference failed to improve predictive value for metabolic syndrome among the Japanese population.

CRP and HMW-adiponectin are both well-known markers for metabolic syndrome, type 2 diabetes and CVD in various ethnics including Japanese [3,4,5,6,7,8,9,10,11]. In this study, we also showed that higher CRP and lower HMW-adiponectin were associated with future development of metabolic syndrome defined by either modified NCEP criteria or JASSO criteria. However, the association between metabolic syndrome and CRP, but not HMW-adiponectin, was markedly attenuated after adjustment for age, sex and BMI or waist circumference. It has been reported that CRP is more closely correlated with obesity than metabolic syndrome [21,22,23]. Our findings also suggested that the association between CRP and metabolic syndrome are largely explained by obesity.

On the other hand, the association between HMW-adiponectin and metabolic syndrome was significant independently of BMI or waist circumference. Adiponectin is an adipokine secreted from adipose tissue and negatively correlated with visceral obesity and presence of CVD [5,6,8,9,10,11]. In animal studies adiponectin has been shown to ameliorate metabolic parameters and suppress progression of atherosclerosis [24]. Specifically, we have shown, as well as others in the field that HMW-adiponectin is a more sensitive marker for metabolic syndrome [16,17,18,25] and type 2 diabetes [26,27] than total adiponectin. However, the usefulness of HMW-adiponectin for prediction of metabolic syndrome compared with the traditional markers remains uncertain. In this study, the predictive value of HMW-adiponectin for metabolic syndrome by ROC analysis was not significantly greater than that of BMI or waist circumference and adding HMW-adiponectin to BMI or waist circumference did not improve predictive ability, suggesting the lack of utility of HMW-adiponectin to predict future development of metabolic syndrome.

In this study, we further investigated the utility of combination of CRP and HMW-adiponectin for predicting metabolic syndrome. Tabara et al. have reported the synergistic effect of CRP and HMW-adiponectin for prediction of metabolic syndrome in a general population [28]. On the other hand, we and others have previously reported that C/A ratio did not improve the predictive ability for metabolic syndrome compared with each of them alone [13,29]. Recently, Ong et al. have reported that CRP and total

Table 3. Odds ratios (95% CI) according to univariate and multivariate logistic regression analyses of HMW-adiponectin and CRP for development of metabolic syndrome.

	MetS			JMetS		
	Univariate	Multivariate		Univariate	Multivariate	
Variable		Model 1	Model 2		Model 1	Model 2
Age (years)	1.05 (1.01–1.09)**	1.04 (1.00–1.08)*	1.03 (0.99–1.07)	1.09 (1.04–1.13)†	1.07 (1.03–1.12)**	1.07 (1.02–1.11)**
Sex (male = 1, female = 0)	1.83 (0.91–3.68)	0.55 (0.24–1.28)	0.60 (0.26–1.36)	6.20 (1.91–20.11)**	0.56 (0.16–1.98)	0.53 (0.15–1.88)
Ln{CRP (mg/L)}	1.54 (1.22–1.96)†	1.21 (0.92–1.59)	1.21 (0.92–1.59)	1.65 (1.28–2.13)†	1.29 (0.95–1.73)	1.26 (0.93–1.71)
Ln{HMW-adiponectin (μg/mL)}	0.45 (0.31–0.64)†	0.60 (0.38–0.96)*	0.56 (0.36–0.88)*	0.33 (0.22–0.49)†	0.50 (0.30–0.81)**	0.48 (0.30–0.78)**
BMI	1.37 (1.25–1.51)†	1.31 (1.18–1.46)†	–	1.36 (1.23–1.50)†	1.25 (1.12–1.39)†	–
Waist circumference (cm)	1.11 (1.07–1.15)†	–	1.09 (1.05–1.13)†	1.13 (1.09–1.17)†	–	1.09 (1.05–1.14)†

CI; confidence interval.
*P<0.05,
**P<0.01,
†P<0.001.
doi:10.1371/journal.pone.0073430.t003

Table 4. Comparison of predictive values of biomarkers for metabolic syndrome.

Variables	AUC of ROC curve (95% CI)	
	MetS	JMetS
CRP (mg/L)	0.646 (0.581–0.711)	0.683 (0.626–0.741)
HMW-adiponectin (ADPN) (μg/mL)	0.674 (0.610–0.738)	0.735 (0.671–0.799)
C/A ratio	0.698 (0.637–0.759)	0.753 (0.699–0.807)
ADPN+CRP	0.690 (0.627–0.752)	0.737 (0.673–0.800)
BMI (kg/m^2)	0.763 (0.711–0.816)	0.758 (0.705–0.811)
Waist circumference (WC) (cm)	0.794 (0.751–0.836)	0.754 (0.703–0.806)
BMI+WC	0.795 (0.751–0.840)	0.763 (0.712–0.814)
BMI+CRP	0.764 (0.712–0.817)	0.761 (0.708–0.813)
BMI+ADPN	0.795 (0.742–0.849)	0.769 (0.717–0.822)
BMI+C/A ratio	0.770 (0.719–0.822)	0.762 (0.710–0.814)
BMI+ADPN+CRP	0.795 (0.742–0.849)	0.772 (0.719–0.824)
WC+CRP	0.754 (0.702–0.806)	0.797 (0.755–0.839)
WC+ADPN	0.768 (0.713–0.822)	0.810 (0.761–0.859)
WC+C/A ratio	0.758 (0.707–0.810)	0.800 (0.759–0.842)
WC+ADPN+CRP	0.768 (0.714–0.823)	0.810 (0.761–0.859)

AUC; area under the curve, ROC; receiver operating characteristics, CI; confidence interval, C/A ratio; CRP to HMW-adiponectin ratio. Lines with variables written with "+" signs indicate that the ROC given is a measure of how well the combination of variables listed explain MetS or JMetS, where values closer to 1 indicate better explanation.

doi:10.1371/journal.pone.0073430.t004

adiponectin levels independently predict the deterioration of glycemia [30]. However, to our knowledge, there has been no study to investigate the utility of combination of both markers for predicting future development of metabolic syndrome in a longitudinal cohort. In the present study, we demonstrated that there is little additive effect of combination of CRP and HMW-adiponectin or C/A ratio for predicting metabolic syndrome compared with each of them alone.

Finally, we examined the additive effect of these biomarkers on the traditional markers for prediction of metabolic syndrome. As a result, ROC analysis revealed that adding CRP and HMW-adiponectin to the traditional markers did not improve the predictive ability for metabolic syndrome. Recently, it has been reported that inflammatory biomarkers including CRP failed to predict type 2 diabetes after adjustment for the traditional markers such as age, sex, BMI and waist circumference [31,32], whereas Ong et al., have reported that adding CRP and adiponectin to the traditional markers improved predictive ability for deterioration in glycemia, especially in women [30]. Further studies are needed to clarify whether the combination of CRP and HMW-adiponectin improve predictive ability for development of metabolic syndrome and type 2 diabetes.

There are limitations in this study. The relatively small number of subjects who developed metabolic syndrome in this study might reduce the ability to detect a statistical difference among the parameters. However, the high follow-up rate of this study (73%) suggested that the effect of selection bias was low. Second, the proportion of women in this study was relatively small and there were only 10 and 3 women who developed MetS and JMets respectively. Thus our findings in women should be confirmed in future studies with a larger sample size, although we found consistent results when we conducted subanalyses of men and women separately. Third, since the original criteria defined by JASSO is used for the diagnosis of metabolic syndrome in Japan, our findings may not apply to other countries or ethnicities which use different criteria of metabolic syndrome. However, we confirmed the findings by use of two different definitions of metabolic syndrome in this study. As we focused to the development of metabolic syndrome in this study, we were not able to exclude the possibility that CRP and HMW-adiponectin may be useful to predict each component of metabolic syndrome such as impaired glucose tolerance and dyslipidemia. Finally, since our study population was limited to healthy middle-aged Japanese (i.e., teachers and workers at University), the results of this study may not be applied to other population such as children and adolescents, and particularly elderly in which the higher adiponectin levels have been shown to associate with higher risk of CVD and mortality [33,34,35,36].

In conclusion, in this study we reported that CRP, HMW-adiponectin or the combination of both did not improve the predictive value of BMI and waist circumference for metabolic syndrome. Our findings indicate that the traditional markers of adiposity such as BMI or waist circumference are still superior markers for predicting metabolic syndrome among the Japanese population.

Supporting Information

Table S1 Odds ratios (95% CI) according to multivariate logistic regression analyses of HMW-adiponectin and CRP for development of metabolic syndrome.
(DOC)

Table S2 Comparison of predictive values of biomarkers for metabolic syndrome in men.
(DOC)

Table S3 Comparison of predictive values of biomarkers for metabolic syndrome in women.
(DOC)

Author Contributions

Conceived and designed the experiments: YS HH HK HI. Performed the experiments: YS HH. Analyzed the data: YS HH TA RR. Contributed reagents/materials/analysis tools: YS HH TA RR. Wrote the paper: YS. Interpretation of the data: YS HH RR TA HK HI. Reviewed/edited the manuscript: YS HH RR TA HK HI. Final approval of the version to be published: YS HH RR TA HK HI.

References

1. Alberti KG, Eckel RH, Grundy SM, Zimmet PZ, Cleeman JI, et al. (2009) Harmonizing the metabolic syndrome: a joint interim statement of the International Diabetes Federation Task Force on Epidemiology and Prevention; National Heart, Lung, and Blood Institute; American Heart Association; World Heart Federation; International Atherosclerosis Society; and International Association for the Study of Obesity. Circulation 120: 1640–1645.
2. Esposito K, Chiodini P, Colao A, Lenzi A, Giugliano D (2012) Metabolic syndrome and risk of cancer: a systematic review and meta-analysis. Diabetes Care 35: 2402–2411.
3. Visser M, Bouter LM, McQuillan GM, Wener MH, Harris TB (1999) Elevated C-reactive protein levels in overweight and obese adults. JAMA 282: 2131–2135.
4. Ford ES (2003) The metabolic syndrome and C-reactive protein, fibrinogen, and leukocyte count: findings from the Third National Health and Nutrition Examination Survey. Atherosclerosis 168: 351–358.

5. Yatagai T, Nagasaka S, Taniguchi A, Fukushima M, Nakamura T, et al. (2003) Hypoadiponectinemia is associated with visceral fat accumulation and insulin resistance in Japanese men with type 2 diabetes mellitus. Metabolism 52: 1274–1278.
6. Matsushita K, Yatsuya H, Tamakoshi K, Wada K, Otsuka R, et al. (2006) Comparison of circulating adiponectin and proinflammatory markers regarding their association with metabolic syndrome in Japanese men. Arterioscler Thromb Vasc Biol 26: 871–876.
7. Corrado E, Rizzo M, Coppola G, Fattouch K, Novo G, et al. (2010) An update on the role of markers of inflammation in atherosclerosis. J Atheroscler Thromb 17: 1–11.
8. Lindsay RS, Funahashi T, Hanson RL, Matsuzawa Y, Tanaka S, et al. (2002) Adiponectin and development of type 2 diabetes in the Pima Indian population. Lancet 360: 57–58.
9. Daimon M, Oizumi T, Saitoh T, Kameda W, Hirata A, et al. (2003) Decreased serum levels of adiponectin are a risk factor for the progression to type 2 diabetes in the Japanese Population: the Funagata study. Diabetes Care 26: 2015–2020.
10. Pischon T, Girman CJ, Hotamisligil GS, Rifai N, Hu FB, et al. (2004) Plasma adiponectin levels and risk of myocardial infarction in men. JAMA 291: 1730–1737.
11. Inoue T, Kotooka N, Morooka T, Komoda H, Uchida T, et al. (2007) High molecular weight adiponectin as a predictor of long-term clinical outcome in patients with coronary artery disease. Am J Cardiol 100: 569–574.
12. Ministry of Health, Labor and Welfare (Japan) (2007) National Health and Nutrition Survey.
13. Saisho Y, Hirose H, Seino Y, Saito I, Itoh H (2010) Usefulness of C-Reactive Protein to High-Molecular-Weight Adiponectin Ratio to Predict Insulin Resistance and Metabolic Syndrome in Japanese Men. J Atheroscler Thromb 17: 944–952.
14. Matthews DR, Hosker JP, Rudenski AS, Naylor BA, Treacher DF, et al. (1985) Homeostasis model assessment: insulin resistance and beta-cell function from fasting plasma glucose and insulin concentrations in man. Diabetologia 28: 412–419.
15. Nakano Y, Tajima S, Yoshimi A, Akiyama H, Tsushima M, et al. (2006) A novel enzyme-linked immunosorbent assay specific for high-molecular-weight adiponectin. J Lipid Res 47: 1572–1582.
16. Seino Y, Hirose H, Saito I, Itoh H (2007) High molecular weight multimer form of adiponectin as a useful marker to evaluate insulin resistance and metabolic syndrome in Japanese men. Metabolism 56: 1493–1499.
17. Seino Y, Hirose H, Saito I, Itoh H (2009) High-molecular-weight adiponectin is a predictor of progression to metabolic syndrome: a population-based 6-year follow-up study in Japanese men. Metabolism 58: 355–360.
18. Hirose H, Yamamoto Y, Seino-Yoshihara Y, Kawabe H, Saito I (2010) Serum high-molecular-weight adiponectin as a marker for the evaluation and care of subjects with metabolic syndrome and related disorders. J Atheroscler Thromb 17: 1201–1211.
19. Alberti KG, Zimmet P, Shaw J (2006) Metabolic syndrome–a new world-wide definition. A Consensus Statement from the International Diabetes Federation. Diabet Med 23: 469–480.
20. The Examination Committee for Criteria of Metabolic Syndrome (2005) Definition and criteria of metabolic syndrome. J Jpn Soc Intern Med 94: 794–809 (in Japanese).
21. Kahn SE, Zinman B, Haffner SM, O'Neill MC, Kravitz BG, et al. (2006) Obesity is a major determinant of the association of C-reactive protein levels and the metabolic syndrome in type 2 diabetes. Diabetes 55: 2357–2364.
22. Timpson NJ, Lawlor DA, Harbord RM, Gaunt TR, Day IN, et al. (2005) C-reactive protein and its role in metabolic syndrome: mendelian randomisation study. Lancet 366: 1954–1959.
23. Aronson D, Bartha P, Zinder O, Kerner A, Markiewicz W, et al. (2004) Obesity is the major determinant of elevated C-reactive protein in subjects with the metabolic syndrome. Int J Obes Relat Metab Disord 28: 674–679.
24. Yamauchi T, Kamon J, Waki H, Imai Y, Shimozawa N, et al. (2003) Globular adiponectin protected ob/ob mice from diabetes and ApoE-deficient mice from atherosclerosis. J Biol Chem 278: 2461–2468.
25. Hara K, Horikoshi M, Yamauchi T, Yago H, Miyazaki O, et al. (2006) Measurement of the high-molecular weight form of adiponectin in plasma is useful for the prediction of insulin resistance and metabolic syndrome. Diabetes Care 29: 1357–1362.
26. Aso Y, Yamamoto R, Wakabayashi S, Uchida T, Takayanagi K, et al. (2006) Comparison of serum high-molecular weight (HMW) adiponectin with total adiponectin concentrations in type 2 diabetic patients with coronary artery disease using a novel enzyme-linked immunosorbent assay to detect HMW adiponectin. Diabetes 55: 1954–1960.
27. Basu R, Pajvani UB, Rizza RA, Scherer PE (2007) Selective downregulation of the high molecular weight form of adiponectin in hyperinsulinemia and in type 2 diabetes: differential regulation from nondiabetic subjects. Diabetes 56: 2174–2177.
28. Tabara Y, Osawa H, Kawamoto R, Tachibana-Iimori R, Yamamoto M, et al. (2008) Reduced high-molecular-weight adiponectin and elevated high-sensitivity C-reactive protein are synergistic risk factors for metabolic syndrome in a large-scale middle-aged to elderly population: the Shimanami Health Promoting Program Study. J Clin Endocrinol Metab 93: 715–722.
29. Devaraj S, Swarbrick MM, Singh U, Adams-Huet B, Havel PJ, et al. (2008) CRP and adiponectin and its oligomers in the metabolic syndrome: evaluation of new laboratory-based biomarkers. Am J Clin Pathol 129: 815–822.
30. Ong KL, Tso AW, Xu A, Law LS, Li M, et al. (2011) Evaluation of the combined use of adiponectin and C-reactive protein levels as biomarkers for predicting the deterioration in glycaemia after a median of 5.4 years. Diabetologia 54: 2552–2560.
31. Chao C, Song Y, Cook N, Tseng CH, Manson JE, et al. (2010) The lack of utility of circulating biomarkers of inflammation and endothelial dysfunction for type 2 diabetes risk prediction among postmenopausal women: the Women's Health Initiative Observational Study. Arch Intern Med 170: 1557–1565.
32. Dallmeier D, Larson MG, Wang N, Fontes JD, Benjamin EJ, et al. (2012) Addition of inflammatory biomarkers did not improve diabetes prediction in the community: the framingham heart study. J Am Heart Assoc 1: e000869.
33. Wannamethee SG, Whincup PH, Lennon L, Sattar N (2007) Circulating adiponectin levels and mortality in elderly men with and without cardiovascular disease and heart failure. Arch Intern Med 167: 1510–1517.
34. Kizer JR, Benkeser D, Arnold AM, Mukamal KJ, Ix JH, et al. (2012) Associations of total and high-molecular-weight adiponectin with all-cause and cardiovascular mortality in older persons: the Cardiovascular Health Study. Circulation 126: 2951–2961.
35. Kizer JR, Benkeser D, Arnold AM, Djousse L, Zieman SJ, et al. (2013) Total and high-molecular-weight adiponectin and risk of coronary heart disease and ischemic stroke in older adults. J Clin Endocrinol Metab 98: 255–263.
36. Saito I, Yamagishi K, Chei CL, Cui R, Ohira T, et al. (2013) Total and high molecular weight adiponectin levels and risk of cardiovascular disease in individuals with high blood glucose levels. Atherosclerosis Epub ahead of print.

Change in β-Cell Mass in Japanese Nondiabetic Obese Individuals

Kinsei Kou, Yoshifumi Saisho, Seiji Satoh, Taketo Yamada, and Hiroshi Itoh

Departments of Internal Medicine (K.K., Y.S., S.S., H.I.) and Pathology (T.Y.), Keio University School of Medicine, Tokyo 160–8582, Japan

Aim: The aim of this study was to clarify the change in β-cell mass in Japanese obese individuals.

Methods: We obtained the pancreas at autopsy from 39 lean and 33 obese Japanese nondiabetic individuals (aged 47 ± 13 vs 47 ± 12 y, $P = .83$, body mass index 20.4 ± 1.6 vs 28.5 ± 3.9 kg/m^2, $P < .01$). Pancreatic sections were stained for insulin, and β-cell area (%BCA) was measured as the fraction of the β-cell area to the total pancreas area. β-Cell mass was then calculated as the product of %BCA and estimated pancreas weight. β-Cell replication and apoptosis were assessed by double staining for insulin and Ki67 and insulin and single-stranded DNA, respectively. The frequencies of insulin-positive duct cells and scattered β-cells were assessed as the surrogate markers of β-cell neogenesis. The α-cell area (%ACA) was also measured, and the %ACA to %BCA ratio was determined.

Results: There was no increase in β-cell mass in obese individuals compared with lean individuals (0.6 ± 0.4 vs 0.7 ± 0.4 g, $P = .12$). β-Cell replication, β-cell neogenesis, and β-cell apoptosis were not significantly increased in the presence of obesity. There was no significant difference in %ACA to %BCA ratio between obese and lean individuals (0.91 ± 1.09 vs 0.75 ± 0.51, $P = .47$).

Conclusion: There was no increase in β-cell mass and no detectable change in β-cell turnover in Japanese obese individuals. ***(J Clin Endocrinol Metab* 98: 3724–3730, 2013)**

Type 1 and type 2 diabetes are both characterized by a deficit of β-cell mass (BCM) (1–6). Preservation or recovery of BCM is therefore an important therapeutic strategy for both type 1 and type 2 diabetes. However, the physiological changes in BCM prior to the development of diabetes remain unclear.

Insulin secretion increases in the face of obesity to compensate insulin resistance (7). Although an increase in BCM has been reported in obese individuals (4, 8), there are no data available on Japanese individuals. There has been one report from Korea showing a positive correlation between fractional β-cell area and body mass index (BMI); however, the positive correlation was seen in only a small number of nondiabetic subjects (2). Recent studies have shown that insulin secretion in Japanese is lower than that in Caucasians (9–11), suggesting that the physiological response of BCM may also differ between Japanese and Caucasians. Therefore, in this study we sought to address the following questions: 1) is BCM increased in Japanese obese individuals; 2) is there any change in β-cell turnover in Japanese obese individuals; and 3) does α-cell area to β-cell area ratio change in Japanese obese individuals?

Materials and Methods

Subjects

Specimens of pancreas obtained at autopsy were obtained with the permission of the bereaved families. The Keio University School of Medicine Review Board approved this study.

Potential cases were first identified by retrospective analysis of the Keio University autopsy database. To be included, cases were required to have the following characteristics: 1) been aged

ISSN Print 0021-972X ISSN Online 1945-7197
Printed in U.S.A.

Received February 11, 2013. Accepted June 6, 2013.
First Published Online June 13, 2013

For editorial see page 3595

Abbreviations: %ACA, fractional α-cell area; %BCA, fractional β-cell area; BCM, β-cell mass; BMI, body mass index; HbA1c, glycated hemoglobin; ssDNA, single-stranded DNA.

Table 1. Characteristics of Subjects

	Total	Lean (BMI < 25 kg/m^2)	Obese (BMI ≥ 25 kg/m^2)	*P* Value
n	72	39	33	
Sex (male/female)	46/26	22/17	24/9	.23
Age, y	47 ± 12 (22–69)	47 ± 13 (22–69)	47 ± 12 (23–69)	.83
Height, cm	165 ± 9 (150–182)	164 ± 9 (150–182)	167 ± 9 (150–182)	.24
Weight, kg	66 ± 17 (44–132)	55 ± 6 (44–74)	80 ± 15 (58–132)	<.01
BMI, kg/m^2	24.1 ± 5.0 (16.1–44.3)	20.4 ± 1.6 (16.1–24.1)	28.5 ± 3.9 (25.2–44.3)	<.01

Data are expressed as mean ± SD (range).

20–69 years; 2) had a full autopsy within 24 hours of death; 3) medical information prior to death; 4) no history of diabetes, pancreatitis, or pancreatic surgery; 5) no use of glucocorticoids; and 6) pancreatic tissue stored that was of adequate size and quality. Cases were excluded if pancreatic tissue had undergone autolysis. As a result, we reviewed approximately 1000 autopsy cases between 1999 and 2011, and 72 cases were found to be eligible for this study. Most (n = 65) specimens were sampled from the body or tail portion of the pancreas and 7 specimens were sampled from the head of the pancreas. The characteristics of the cases are summarized in Table 1, with causes of death in Supplemental Table 1, published on The Endocrine Society's Journals Online web site at http://jcem.endojournals.org.

Cases were divided into 39 lean [body mass index (BMI) < 25 kg/m^2] and 33 obese (BMI ≥ 25 kg/m^2) cases according to the definition of obesity by the Japan Society for the Study of Obesity (12).

Pancreatic tissue processing

The pancreas was fixed in formaldehyde at autopsy and then embedded in paraffin for subsequent analysis. Then 5-μm sections were stained for light microscopy as follows: 1) with hematoxylin-eosin, 2) for insulin (peroxidase staining) with hematoxylin, 3) for glucagon with hematoxylin, 4) for insulin and Ki67 for assessment of β-cell replication, and 5) for insulin and single-stranded DNA (ssDNA) for assessment of β-cell apoptosis (13–15). For immunohistochemical staining, guinea pig polyclonal antibodies against porcine insulin and rabbit polyclonal antibodies against human glucagon were used (DAKO Japan, Kyoto, Japan). Furthermore, rabbit polyclonal antibodies against ssDNA (IBL, Takasaki, Japan) and murine monoclonal antibodies against human Ki67 (DAKO Japan) were used for the detection of apoptotic cells and proliferating cells, respectively. β-Cell apoptosis was also assessed by rabbit polyclonal antibodies against large fragment (17/19 kDa) of cleaved caspase-3 (Cell Signaling Technology, Boston, Massachusetts) and rabbit polyclonal antibodies against large fragment (89 kDa) of cleaved human poly(ADP-ribose) polymerase-1 (Cell Signaling Technology).

Morphometric analysis

To quantify fractional β-cell area (%BCA), the entire pancreatic section (219 ± 93 mm^2) was imaged at ×200 magnification (×20 objective) using a Mirax Scan and Mirax Viewer (Carl Zeiss MicroImaging GmbH, Goettingen, Germany). The ratio of β-cell area to total pancreas area was digitally measured using Image Pro Plus software (Media Cybernetics, Silver Spring, Maryland) as previously reported (8). Interlobular connective tissue, large blood vessels, and adipocytes were excluded from total pancreas area; thus, total pancreas area consisted to the greatest extent of pancreatic acinar tissue and pancreatic islets. Likewise, the ratio of α-cell area to total pancreas area (%ACA) was also digitally measured, and the ratio of %ACA to %BCA was determined in each case. All measurements were conducted by a single investigator (K.K.), and intraobserver coefficient of variance (computed in 5 cases studied on 5 occasions) was 7%. All measurements were conducted twice, and the mean of the 2 measurements was used. At the measurement the investigator was blinded to the BMI status of each specimen. In a preliminary analysis, the measurements of the %BCA independently assessed by 2 investigators (K.K. and Y.S.) were sufficiently comparable ($n = 51, r = 0.9, P < .01$, y (percentage) = 1.04x (percentage) + 0.1). Interobserver variance was about 12%.

To measure individual β-cell size, 6 islets per case were selected at random using a Mirax Viewer (Carl Zeiss MicroImaging). These islets were then examined to identify 6 representative β-cells in each. Selection criteria included a circular shape (similar dimensions in all directions) and the appearance to the observer that the cell had been sectioned through its maximum diameter. For the determination of the mean cell diameter, 6 distances between 2 adjacent β-cell nuclei (including one of the nuclei) were measured in each of the 6 islets (ie, total of 36 diameters in each case). The β-cell size was determined as mean β-cell diameter.

To conduct further morphometric analysis, scattered β-cells, insulin-positive duct cells, β-cell replication, and apoptosis were quantified in randomly selected areas of the pancreas (26.2 ± 13.5 mm^2) that contained more than 100 islets in each case, using a Mirax Viewer (Carl Zeiss MicroImaging). Scattered β-cells were defined as a cluster of three or fewer β-cells in acinar tissue, and the density of scattered β-cells was determined as the number of scattered β-cells/pancreas area (square millimeters). Insulin-positive duct cells were also counted and expressed as the number of insulin-positive duct cells/pancreas area (square millimeters). β-Cell replication and apoptosis were quantified, and the frequencies of β-cell replication and apoptosis were expressed as percentage of islets. A total of 7778 islets (108 ± 7 islets per section) were assessed for these analyses.

Pancreas parenchymal volume

Because pancreas weight was not available in most cases, to determine BCM, the pancreas parenchymal volume was estimated using equations based on population data described in detail elsewhere (16). Briefly, the pancreas parenchymal volume increases in childhood to reach a plateau at age 20 years. From age 20–60 years, pancreas parenchymal volume is stable and is described as a function of obesity. Thus, we estimated pancreas parenchymal volume of each autopsy case using the equation: $y^P = 34.6 + 0.55x$ [y^P: pancreas parenchymal volume (cubic centimeters), x: BMI].

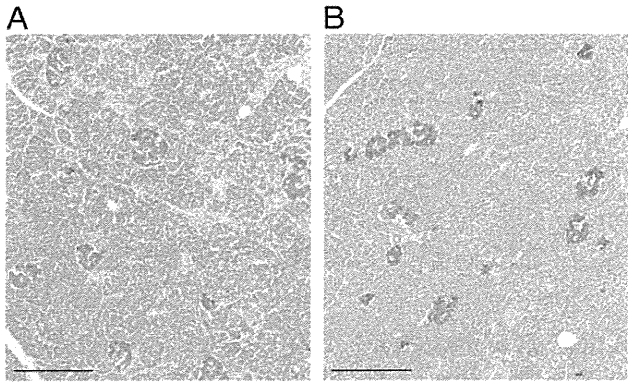

Figure 1. Representative photomicrographs of pancreas immunostained for insulin (brown) and with hematoxylin (×20 objective). No increase in β-cell area was observed in an obese individual (43 y old man, BMI 26.1 kg/m^2; B) compared with a lean individual (49 y old man, BMI 18.3 kg/m^2; A). Scale bar, 300 μm.

Assessment of β-cell mass

BCM was calculated as the product of %BCA, determined by immunohistochemical staining in each individual, and estimated pancreas parenchymal weight, determined as above (assuming 1 g of weight per 1 cm^3 pancreas volume).

Statistical analysis

Data are presented as mean ± SD in the text and tables and mean ± SEM in the figures. Statistical comparisons were carried out using a Student's *t* test, with a $P < .05$ taken as significant. Simple regression was carried out for correlation analysis.

Results

β-Cell mass in obesity

Representative pictures of the pancreas in lean and obese individuals are shown in Figure 1. The %BCA in obese subjects was significantly decreased compared with that in lean subjects (1.14 ± 0.81 vs 1.57 ± 0.84%, $P = .03$, Figure 2A). There was a significant negative correlation between β-cell area and BMI ($r = -0.25$, $P = .04$, Figure 2B), although the range of β-cell area largely overlapped between lean and obese subjects. Based on the population data, the pancreas parenchymal volume was estimated to be approximately 10% greater in obese subjects than in lean subjects (50.3 ± 2.2 vs 45.8 ± 1.0 cm^3, $P < .01$). Despite the greater pancreas volume in obese subjects, BCM, which was a product of %BCA, and the estimated pancreas parenchymal volume (assuming 1 g of weight per 1 cm^3 pancreas parenchymal volume) remained lower in obese subjects than in lean subjects, although the difference was not statistically significant (0.57 ± 0.40 vs 0.72 ± 0.38 g, $P = .12$, Figure 2C). There was no significant correlation between BCM and BMI ($r = -0.16$, $P = .19$, Figure 2D).

To exclude possible confounding factors, we conducted several subanalyses. After excluding subjects who died from malignancy, we confirmed no increase in %BCA and BCM in obese compared with lean subjects ($n = 29$, 0.80 ± 0.12 vs 1.63 ± 0.30%, $P = .01$ and 0.40 ± 0.06 vs 0.74 ± 0.14 g, $P = .03$, respectively). Similarly, after excluding subjects whose samples were obtained from the pancreatic head, there was no increase in %BCA and BCM in obese compared with lean subjects ($n = 65$, 1.13 ± 0.13 vs 1.63 ± 0.14%, $P = .01$, and 0.57 ± 0.07 vs 0.74 ± 0.06 g, $P = .06$). Finally, the results were also the same in subjects aged 60 years or less ($n = 66$, %BCA: 1.16 ± 0.15 vs 1.52 ± 0.14%, $P = .08$, and BCM: 0.58 ± 0.08 vs 0.70 ± 0.06 g, $P = .25$, in obese vs lean subjects, respectively). There was no correlation between age and %BCA or BCM ($r = -0.21$, $P = .09$ and $r = -0.12$, $P = .34$).

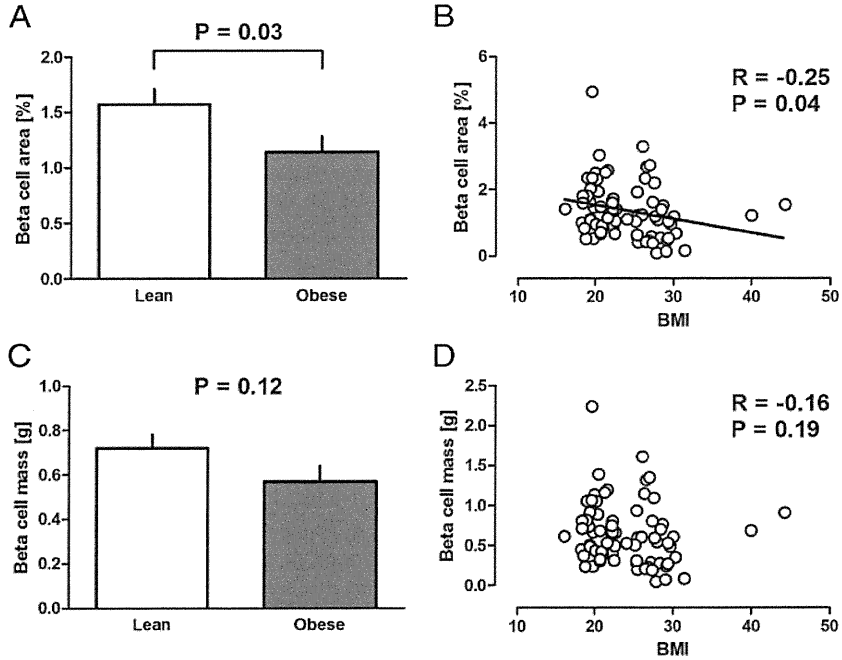

Figure 2. The %BCA and BCM in relation to obesity in Japanese individuals. The %BCA was significantly decreased in obese subjects compared with lean subjects (A), and there was a significant negative correlation between %BCA and BMI (B). After adjustment for pancreas volume, the estimated BCM in obese subjects was not significantly different from that in lean subjects (C). There was no significant correlation between BCM and BMI (D).

β-Cell turnover in obesity

Individual β-cell size determined as β-cell diameter was not significantly different between lean and obese subjects (8.53 ± 0.72 vs